

Review

# ATP Analogues for Structural Investigations: Case Studies of a DnaB Helicase and an ABC Transporter

Denis Lacabanne <sup>1,2,†</sup>, Thomas Wiegand <sup>1,\*,†</sup> , Nino Wili <sup>1</sup> , Maria I. Kozlova <sup>3</sup> ,  
Riccardo Cadalbert <sup>1</sup>, Daniel Klose <sup>1</sup>, Armen Y. Mulkidjanian <sup>3,4</sup>, Beat H. Meier <sup>1,\*</sup> and  
Anja Böckmann <sup>5,\*</sup>

<sup>1</sup> Laboratory of Physical Chemistry, ETH Zurich, 8093 Zurich, Switzerland;

denis.lacabanne@mrc-mbu.cam.ac.uk (D.L.); nino.wili@phys.chem.ethz.ch (N.W.);

Riccardo.Cadalbert@nmr.phys.chem.ethz.ch (R.C.); daniel.klose@phys.chem.ethz.ch (D.K.)

<sup>2</sup> Medical Research Council Mitochondrial Biology Unit University of Cambridge,

Cambridge Biomedical Campus, Keith Peters Building, Hills Road, Cambridge CB2 0XY, UK

<sup>3</sup> Department of Physics, Osnabrueck University, 49069 Osnabrueck, Germany;

makozlova@uni-osnabrueck.de (M.I.K.); armen.mulkidjanian@uni-osnabrueck.de (A.Y.M.)

<sup>4</sup> School of Bioengineering and Bioinformatics and Belozersky Institute of Physico-Chemical Biology,

Lomonosov Moscow State University, 119234 Moscow, Russia

<sup>5</sup> Molecular Microbiology and Structural Biochemistry UMR 5086 CNRS/Université de Lyon, Labex Ecofect,  
69367 Lyon, France

\* Correspondence: thomas.wiegand@phys.chem.ethz.ch (T.W.); beme@ethz.ch (B.H.M.); bockmann@ibcp.fr (A.B.)

† These authors contributed equally to this work.

Academic Editor: Marilisa Leone

Received: 17 October 2020; Accepted: 9 November 2020; Published: 12 November 2020



**Abstract:** Nucleoside triphosphates (NTPs) are used as chemical energy source in a variety of cell systems. Structural snapshots along the NTP hydrolysis reaction coordinate are typically obtained by adding stable, nonhydrolyzable adenosine triphosphate (ATP) -analogues to the proteins, with the goal to arrest a state that mimics as closely as possible a physiologically relevant state, e.g., the pre-hydrolytic, transition and post-hydrolytic states. We here present the lessons learned on two distinct ATPases on the best use and unexpected pitfalls observed for different analogues. The proteins investigated are the bacterial DnaB helicase from *Helicobacter pylori* and the multidrug ATP binding cassette (ABC) transporter BmrA from *Bacillus subtilis*, both belonging to the same division of P-loop fold NTPases. We review the magnetic-resonance strategies which can be of use to probe the binding of the ATP-mimics, and present carbon-13, phosphorus-31, and vanadium-51 solid-state nuclear magnetic resonance (NMR) spectra of the proteins or the bound molecules to unravel conformational and dynamic changes upon binding of the ATP-mimics. Electron paramagnetic resonance (EPR), and in particular W-band electron-electron double resonance (ELDOR)-detected NMR, is of complementary use to assess binding of vanadate. We discuss which analogues best mimic the different hydrolysis states for the DnaB helicase and the ABC transporter BmrA. These might be relevant also to structural and functional studies of other NTPases.

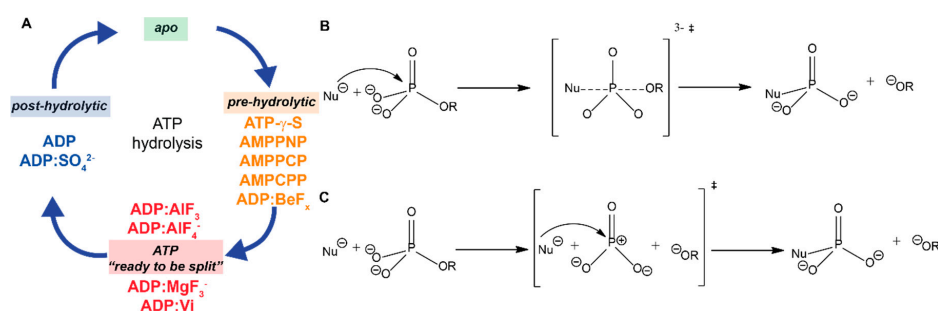
**Keywords:** solid-state NMR; ELDOR-detected NMR; ATP hydrolysis; ATP analogues; DnaB helicase; ABC transporter

## 1. Introduction

Nucleosides triphosphates (NTPs), such as ATP (adenosine triphosphate) and GTP (guanosine triphosphate), are used as energy source or as allosteric effector by a number of proteins, involved for instance, in metabolism, active transport, cell division or DNA/RNA synthesis. However, the mechanism of NTP hydrolysis in proteins are still poorly understood, especially its coupling to

functional events, such as movement of proteins along nucleic acids. Indeed, detailed mechanistic insight is lacking for a number of systems, including even intensively studied systems such as dyneins [1], ABC importers [2]/exporters [3] or DNA helicases [4]. Experimentally, catching the events that occur during the NTP hydrolysis is highly challenging. Structural techniques such as X-ray crystallography, cryo-electron microscopy (cryo-EM) and nuclear magnetic resonance (NMR) mainly provide static snapshots of protein states of typically highly complex reaction coordinates of biomolecular reactions. These can then be combined with molecular dynamics simulations (MD) to obtain further information about the dynamics of such processes and to establish the chronological sequence [3,5–8]. In this context, it is highly desirable to better investigate how ATP/GTP analogues, usually with a modified or replaced  $\gamma$ -phosphate group, can mimic the intermediate catalytic states in order to obtain relevant snapshots of the reactions involving NTP hydrolysis. Indeed, it is well known that mimics can never fully represent naturally occurring states, as the modifications of NTPs change their conformation as well as their chemical properties other than their tendency to hydrolyse. While it is important to use NTP mimics described to be strongly hydrolysis-resistant, the true hydrolysis state must often be confirmed experimentally.

The choice of the adequate analogue is thus of importance in structural studies, but guidelines are sparse and can be highly protein-dependent. We herein focus on analogues often used to access three important states of ATP-hydrolysis: the pre-hydrolytic state, the transition state and the post-hydrolytic state (see Scheme 1A for the artificial ATP hydrolysis scheme highlighting analogues used to mimic the different states). We describe how NMR and EPR can be used to gain detailed information on the analogue used and the conformational and dynamic state it induces in the protein. We investigate this for two proteins, the bacterial DnaB helicase from *Helicobacter pylori* involved in DNA replication, and an ABC transporter implicated in multidrug resistance, BmrA (*Bacillus subtilis* multidrug resistance ATP binding cassette transporter), which share high similarities in their ATP binding sites [9]. Solid-state NMR and EPR are highly suitable to study large, noncrystalline protein assemblies, which are represented by DnaB and BmrA. The proteins are, in their multimeric states and, for BmrA, embedded in a *Bacillus subtilis* lipid membrane, sedimented directly into the solid-state NMR rotor in an external ultracentrifuge [10], a sample preparation approach that allows for the study of the investigated analogues. The protein samples prepared by this approach are highly concentrated in the NMR rotor (protein concentration of around 400 mg/mL), and have been shown to be stable over several years [11]. A description of the NMR techniques developed to investigate such molecular machines is given in detail in reference [12].



**Scheme 1.** Artificial ATP hydrolysis scheme and associative and dissociative mechanism of ATP hydrolysis. (A) Artificial ATP hydrolysis scheme showing ATP analogues used to mimic the pre-hydrolytic, the “ATP-is-ready-to-be-split” and the post-hydrolytic state. Schematic representation of the associative (B) and dissociative (C) mechanism of ATP hydrolysis. Nu<sup>⊖</sup> represents a nucleotide, e.g., an OH<sup>⊖</sup>.

Figure 1 and Table 1 summarize the most important NMR experiments and the nomenclature used herein and gives the information content of NMR spectra and the underlying NMR observables. The standard experiment to establish a chemical-shift fingerprint of the protein is the <sup>13</sup>C-<sup>13</sup>C DARR, a two-dimensional correlation experiment using the dipolar assisted rotational recoupling (DARR)

scheme [13,14]. Besides delivering a first sample quality check (Figure 1A), isolated peaks in such spectra, often found in the alanine or threonine regions, can serve to follow the conformational changes along the reaction coordinate. Differences in the cross-peak positions (encoding the chemical shift) in such spectra characterize the different protein conformations, produced by incubating the protein with ligands. Such changes are denoted as chemical-shift perturbations (CSPs) (Figure 1B). Additionally, appearing or disappearing resonances might be observed in the spectra, pointing to dynamic changes of the protein (Figure 1C).  $^{31}\text{P}$  NMR experiments allow for direct detection of nucleotides, such as ATP mimics or DNA/RNA [12] (Figure 1D). The  $^{31}\text{P}$  chemical-shift values react very sensitively to small conformational changes, e.g., in the phosphate backbone of ATP mimics.  $^{31}\text{P}$  direct-pulsed experiments (recorded with short repetition times, Figure 1E) are used to detect unbound nucleotides present in the water phase in contact with the protein (interacting water) or the supernatant of the NMR rotor [15].  $^{31}\text{P}$  cross-polarization (CP) based experiments are employed to detect immobilized nucleotides, particularly those bound to the protein (Figure 1E). ELDOR-detected NMR (EDNMR) is a pulsed EPR-technique and allows for the measurement of hyperfine couplings of paramagnetic spin centers to nearby spin-active nuclei [16–19]. We herein use this technique to detect NMR-active nuclei in the vicinity of the ATP-cofactor (for this the diamagnetic  $\text{Mg}^{2+}$  has to be substituted by paramagnetic  $\text{Mn}^{2+}$ ), particularly focusing on  $^{31}\text{P}$  and  $^{51}\text{V}$  nuclear spins [20]. If a  $^{51}\text{V}$  nucleus is in spatial proximity to the  $\text{Mn}^{2+}$  ions, the  $^{51}\text{V}$  resonance should be detected in the EDNMR spectra (Figure 1F). Note that the hyperfine coupling to the  $^{51}\text{V}$  is often not resolved, in contrast to the  $^{31}\text{P}$  couplings.

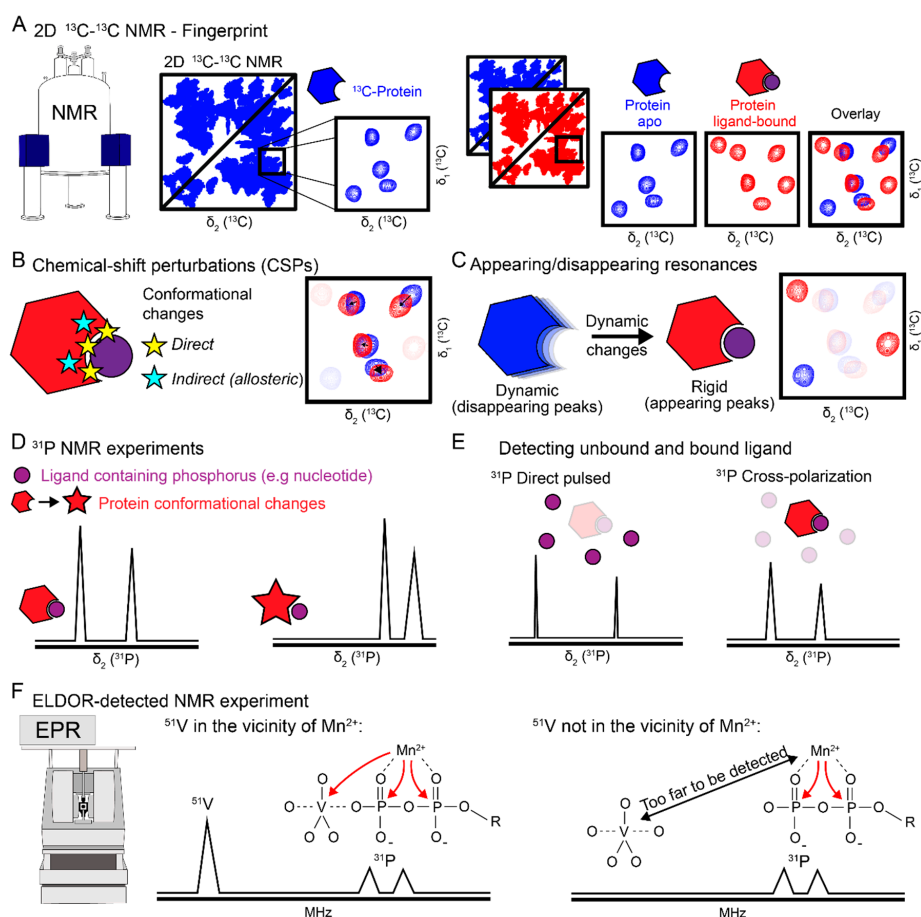


**Figure 1.** Magnetic-resonance approaches used to investigate the helicase DnaB and the ABC transporter BmrA in presence of ATP mimics. The employed techniques comprise 2D  $^{13}\text{C}$ - $^{13}\text{C}$  NMR spectral fingerprints (A),  $^{13}\text{C}$  chemical-shifts perturbations (B), appearing/disappearing resonances due to dynamic changes (C),  $^{31}\text{P}$  NMR experiments (D) to detect bound and unbound ligands (E) and ELDOR-detected NMR experiments (F), Details are given in the text.

**Table 1.** Overview of magnetic-resonance techniques applied in this work and information extracted. A cross indicates that this information is contained in the experimental outcome, a blank indicates that the type of extracted information is not accessible by the experiment.

Magnetic-Resonance Technique	Protein Conformational Changes	Protein Dynamic Changes	Nucleotide Binding	Nucleotide Conformation	Vanadate Binding	Metal Co-Factor Binding
NMR $^{13}\text{C}/^{15}\text{N}$ fingerprints	x	x	x			
CSPs	x		x			
Disappearing/appearing resonances		x	x			
$^{31}\text{P}$ CP-MAS			x			
$^{31}\text{P}$ chemical-shift values			x	x	x	
$^{51}\text{V}$ NMR					x	
EDNMR					x	x

We here make use of these magnetic-resonance approaches to study the states of DnaB and BmrA induced by phosphate-modified NTP analogues widely used to mimic the three major states of the NTP hydrolysis reaction and report on the efficiency of the analogues to actually mimic the desired states.

## 2. The Different Hydrolysis States and the ATP-Mimics Used to Induce Them

The pre-hydrolytic state, where ATP is bound to the protein, is often already associated with protein conformational changes [21–24]. In this state, the  $\gamma$ -phosphate adopts a tetrahedral geometry (note that a similar discussion also holds for GTP). This geometry can change to a trigonal-bipyramidal geometry generating a pentavalent terminal phosphate group [25,26]. Most of the analogues are mimicking the pre-hydrolytic state because their  $\gamma$ -phosphate (in case of nonhydrolyzable analogues) or the  $\gamma$ -phosphate-mimicking group adopts a tetrahedral geometry [27]. The most commonly used nonhydrolyzable analogues are: AMPPNP (adenylyl imidodiphosphate) [28], AMPPCP (adenylyl methylenediphosphate) [29], AMPCPP (alpha,beta-methylene-triphosphonate) and ATP- $\gamma$ -S (adenosine 5'-(gamma-thiotriphosphate)) [30]. In addition, the pre-hydrolytic state appears to be mimicked by ADP-BeF<sub>x</sub> [27] (Figures 2 and 3A). BeF<sub>x</sub> forms a strictly tetrahedral complex (specific to the pre-hydrolytic state); a penta-coordinated bipyramidal geometry (describing the transition state, see below) is excluded in this case [26,27]. The nonhydrolyzable ATP analogues are not completely resistant to hydrolysis. While the rate of hydrolysis of these analogues is indeed significantly lower, several of them can still be hydrolysed by many ATPases [31–38]. This behaviour can differ from protein to protein, and an analogue can fail to mimic a pre-hydrolytic state or may mimic a different/uncomplete pre-hydrolytic state in certain cases [26,39–41]. This difference can be observed between distinct protein families, or even within the same family [42], as shown in this work for the two model systems discussed.

The transition state (the “ATP-is-ready-to-be-split” state) can be accessed by an associative and dissociative mechanism, which represent the two extreme cases discussed in the literature [43–48]. In the case of an associative mechanism, the phosphorus possesses a pentavalent geometry. The nucleophilic attack of a water molecule at the  $\gamma$ -phosphate, forming a H<sub>2</sub>O-P bond, in this scenario occurs before the leaving group departs and before the P-O bond breaks (similar to a S<sub>N</sub>2 nucleophilic substitution, see Scheme 1B,C). In contrast, in the case of a dissociative mechanism, the nucleophilic attack of a water molecule at the  $\gamma$ -phosphate occurs after the leaving group was released, generating a metaphosphate intermediate before it collapses onto the acceptor nucleophile (similar to a S<sub>N</sub>1 reaction). The transition state can be simulated by employing three prominent mimic groups in combination with ATP or ADP: aluminium fluoride (ADP:AlF<sub>x</sub>) [27,49,50], magnesium fluoride (ADP:MgF<sub>x</sub>) [51], and vanadate (ADP:Vi) [52]. In some enzymes, ATP hydrolysis is required prior to the binding of the transition-state mimic [53,54]. In structural studies, aluminium fluoride is most frequently used as a mimic of the  $\gamma$ -phosphate in the transition state, as evidenced by analysing the number of deposited structures in the PDB database (Figure 2A). When the analogue in the presence of ADP is complexed with the protein, ADP:AlF<sub>x</sub> is believed to mimic the transition state of an ATP molecule. Two configurations of this analogue have been observed: ADP:AlF<sub>3</sub> and ADP:AlF<sub>4</sub><sup>−</sup>. In the ADP:AlF<sub>4</sub><sup>−</sup> mimic (two-thirds of in the

PDB deposited  $\text{AlF}_x$ -containing structures) the  $\text{AlF}_4^-$  group is in a squared-planar geometry and forms an octahedral complex with two oxygen ligands in the apical positions. While one ligand is provided by the  $\beta$ -phosphate, the other ligand comes from the hydrolytic water molecule in the attack position next to the phosphorus atom. It is believed that such a structure mimics the interaction of the catalytic water molecule with the  $\gamma$ -phosphate in the anionic transition state for phosphoryl transfer [49,55].  $\text{AlF}_3$  (one-third of in the PDB deposited  $\text{AlF}_x$ -containing structures) is in a trigonal-planar geometry forming a bipyramidal complex resembling the geometry of the transition state [49,55].

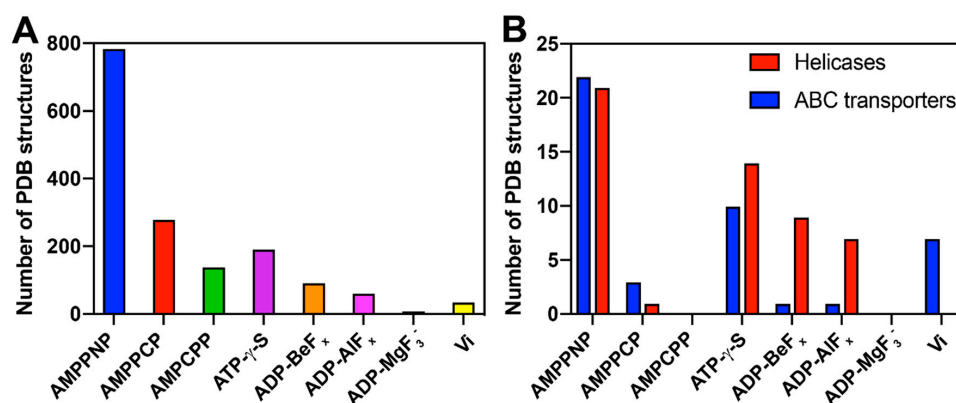


**Figure 2.** Distribution of the different NTP analogues based on the number of structures in the Protein Data Bank in December 2019. Number of Protein Data Bank structures for each analogue (A). Number of ABC transporters (blue, search query “ABC transporter + protein data bank accession codes of the ATP-analogue”) and helicases (red, search query “DNA helicase + PDB ID of the ATP-analogue”) Protein Data Bank structures for each analogue (B).

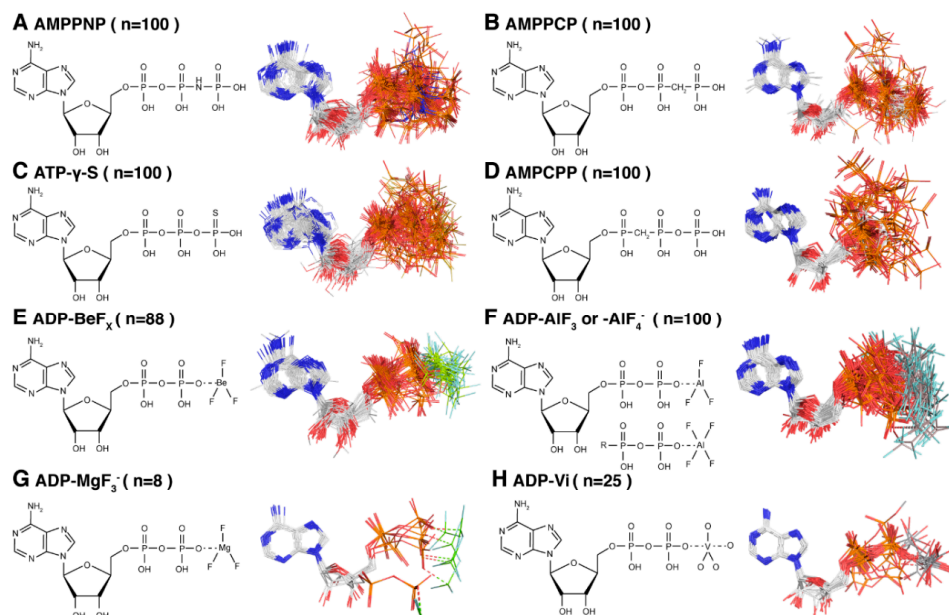


**Figure 3.** ATP analogues mainly used for structure determination. Left panel is the chemical structure and the right panel shows the protein-bound-structure of AMPPNP (A), AMPPCP (B), ATP- $\gamma$ -S (C), AMPCPP (D), ADP:BeF<sub>x</sub> (E), ADP:AlF<sub>x</sub> (F), ADP:MgF<sub>3</sub><sup>-</sup> (G), ADP:Vi (H) from the Protein Data Bank (<https://www.rcsb.org>). The protein-bound-structures of ATP analogues were generated after alignment of their adenosine moieties. In order to compare the molecules among each other, only the first 100 structures with the smallest RMSD were selected for AMPPNP, AMPPCP, ATP- $\gamma$ -S and AMPCPP.

$\text{MgF}_3^-$  shows nearly the same geometry as  $\text{AlF}_3$  but carries a negative charge similarly to the anionic  $\gamma$ -phosphate in the transition state.  $\text{AlF}_3$  and  $\text{MgF}_3^-$  are structurally similar and have similar scattering factors for X-rays; therefore, it has been suggested that  $\text{MgF}_3^-$  is present in some crystal structures, which are indicated as containing  $\text{NDP:AlF}_3$  [56]. Indeed,  $\text{Mg}^{2+}$  ions are usually present in the samples as cofactors of NTP hydrolysis. In contrast to X-ray, NMR can differentiate the two metal fluorides so that in few cases, the presence of  $\text{MgF}_3^-$  in the active site was directly shown [56–58]. For more information about such cases and the use of metal fluorides as ATP or phosphate analogues, we refer the reader to the two comprehensive recent reviews [55,58]. Finally, vanadate-containing ATP:Vi or ADP:Vi are used as a transition-state mimic for a variety of proteins. Vanadate is an oxoanion of vanadium which shares structural and chemical similarities with phosphate molecules mimicking the hydrolysis transition state [52,59]. It is known that the simple form of the oxoanion ( $\text{VO}_4^{3-}$ ) can adopt a penta-coordinated, trigonal bipyramidal geometry around the central vanadium in presence of ADP [60]. These properties make the vanadate a phosphate mimic of the transition state for phosphoryl transfer so that vanadate acts as an inhibitor for some ATPases. As previously described by Davies et al. [52], vanadate can be used to mimic phosphoryl transfer, and structures of different protein families including myosin [61,62], dynein [63], kinesin [40], ABC transporters [60,64,65], heat shock protein (Hsp70s) [66], NS3 helicase (dengue virus) [67], nucleoside-diphosphate kinase [68] or F1-ATPase [69] are reported. The main advantage of vanadate is that it can form covalent bonds with the oxygens of phosphate groups from ADP or other ligands [52]. Interestingly, this is not always the case [68], as there are structures where a vanadate is not bound to ADP, but still stabilizes the transition state. It is also noteworthy that vanadate does not work as an inhibitor or as transition-state mimic for all proteins with ATPase activity [70].

Finally, the post-hydrolytic state corresponds to a situation where the nucleotide diphosphate and the previously associated  $\gamma$ -phosphate are separated, but both are still bound to the protein, or, alternatively, where the  $\gamma$ -phosphate is already released, and only ADP is bound to the protein. The post-hydrolytic state where the  $\gamma$ -phosphate is not released can be mimicked not only by an orthophosphate [67,71,72] but also by a sulphate ion,  $\text{SO}_4^{2-}$  [71,73–75]. Note that sulphate ions have only two ionisable oxygens (with  $\text{pK}_a$  below 2) [76].

The overall conformational variability of NTP analogues can be seen by overlaying the structures extracted from the PDB and by aligning them on their nucleoside parts (Figure 3). AMPPNP and ATP- $\gamma$ -S adopt a wider range of conformations (Figure 3A,C) than AMPPCP and ADP:BeF<sub>x</sub> (Figure 3B,E), although this allows for a qualitative statement only, since the total numbers of deposited structures in the PDB are different (see Figure 2). AMPPNP and ATP- $\gamma$ -S thus seem to adapt their conformation to the protein-binding pocket, while for AMPPCP and ADP:BeF<sub>x</sub> it may be the protein that adapts. For the transition-state analogues, it is difficult to make the same comparison due to the small number of structures available. However, ADP:AlF<sub>x</sub> shows a significant distribution of structures as well (Figure 3F).

In sum, from the eight mainly used analogues for structural studies, five are used to mimic the pre-hydrolytic state: AMPPNP, AMPPCP, ATP- $\gamma$ -S, AMPCPP and ADP:BeF<sub>x</sub>, three to mimic the transition state: ADP:AlF<sub>x</sub>, ADP:MgF<sub>x</sub> and ADP:Vi, and ADP and ADP:SO<sub>4</sub><sup>2-</sup> to mimic the post-hydrolytic state. Note that also other NTP analogues exist that differ structurally through the introduction of atoms or groups (e.g., fluorescent probes, biotin groups, etc.) on the base, sugar, or triphosphate regions of the molecule [77–79]. A complete overview is given in reference [77].

### 3. The DnaB Helicase and the ABC Transporter BmrA

The usefulness of particular ATP mimics for structural studies strongly depends on the nature of the protein of interest, as shown in Figure 2B for the example of DNA helicases and ABC transporters. The two proteins were subject to studies in the last years in our laboratories: the bacterial helicase DnaB from *Helicobacter pylori* [38,80–88] and the ABC transporter BmrA from *Bacillus subtilis* [86,89–92]. In the presence of double-stranded DNA, the DnaB from *Helicobacter pylori* is a double-homo hexamer of

59 kDa monomers with each hexamer moving along its single DNA strand, whereas BmrA from *Bacillus subtilis* is a dimeric membrane protein of 65 kDa monomers. The two proteins are well-characterized ATP-fuelled proteins. In both proteins, the chemical energy released during ATP hydrolysis in the nucleotide-binding domain (NBD) is converted into mechanical work, which, e.g., enables the movement of DnaB along a double-stranded DNA and its unzipping, as well as the transportation of molecules across the membrane by ABC transporters. Both proteins belong to the vast family of P-loop fold NTPases, one of the largest protein superfamilies. In any genome 10–20% of proteins code for P-loop fold domains [93–95]. P-loop fold NTPases are characterized by their signature GxxxxGK [S/T] sequence motif, also known as the Walker A motif [96]. This motif is responsible for binding the triphosphate chain and is often called the P-loop (phosphate-binding loop) motif [97]. In the P-loop fold, the conserved Lys residue forms hydrogen bonds with the  $\beta$ - and  $\gamma$ -phosphate groups of ATP or GTP. Another conserved motif, known as the Walker B motif, is composed of four hydrophobic residues ended by an aspartate residue. The conserved Asp residue stabilizes the metal ion cofactor  $Mg^{2+}$  [96].

The C-terminal NBD of DnaB belongs to the superfamily 4 (SF4) of helicases, which in turn belongs to the class “RecA and  $F_1/F_0$ -related ATPases” (hereafter abbreviated as RecA/ $F_1$ -related ATPases) of P-loop old NTPases. The ABC transporter BmrA belongs to a separate class of ABC transporters [93–95]. Both the RecA/ $F_1$ -related ATPases and ABC transporters belong to the ASCE division of P-loop fold NTPases. The members of this division are characterized by an additional  $\beta$ -strand in the P-loop fold and a catalytic glutamate (E) residue next to the attacking water molecule [94,95,98]. The glutamate residue stabilizes the catalytic water molecule and, perhaps, operates as a catalytic base for ATP hydrolysis [99].

To avoid a futile NTP hydrolysis, P-loop fold NTPases are initiated before each turnover by activating moieties provided either by other proteins or by domains of the same protein [100–104]. The activating moiety interacts with the triphosphate chain and triggers the hydrolysis. The ATP hydrolysis in DnaB is induced by an interaction with an arginine residue that is provided by the neighbouring subunit of the same oligomer [105,106]. In ABC transporters, one of the NBDs is believed to activate hydrolysis within the active site in the other NBD by providing a signature LSGGQ motif [64,106].

Two analogues were mainly used in structural studies of helicases and ABC transporters (Figure 2): AMPPNP and ATP- $\gamma$ -S, which both mimic the pre-hydrolytic state. The transition state is mainly mimicked by ADP:AlF<sub>x</sub> for the helicases, and ADP:Vi for the ABC transporters. Regarding the literature, this state is underrepresented compared to the pre-hydrolytic state.

We here gather information from published experiments, as well as present complementary original data, in order to give a compilation of ATP analogues and their mimicking power for the two proteins DnaB and BmrA, as assessed by magnetic-resonance methods, namely NMR and EPR.

## 4. Results and Discussion

### 4.1. The Pre-Hydrolytic State Mimicked by AMPPCP, AMPPNP and ATP- $\gamma$ -S

In order to characterize the pre-hydrolytic state, we first investigated DnaB and BmrA in the presence of AMPPNP, AMPPCP, and ATP- $\gamma$ -S. It however appeared that ATP- $\gamma$ -S was completely hydrolysed during the rotor filling by BmrA (one hour of filling) and DnaB (overnight filling), as monitored by  $^{31}P$  solid-state NMR experiments (see Figure S1), and was thus of no further use. We therefore focused on AMPPNP and AMPPCP. Since a major function of the DnaB helicase is to bind to DNA, protein samples were also prepared with the ATP analogue and single-stranded DNA (here a DNA-fragment of 20 thymidine nucleotides abbreviated as (dT)<sub>20</sub>). The presence of three signals in the 1D CP  $^{31}P$  NMR spectrum (Figure 4A, left panel) indicates binding of the triphosphate AMPPCP to DnaB. However, the resonances of the phosphorus  $\alpha$  and  $\beta$  are rather broad. This broadening might indicate inhomogeneities in the binding site in the environment of the ligand, or chemical-exchange broadening effects. In contrast, in the presence of DNA and AMPPCP, the  $^{31}P$  resonances in the 1D CP

$^{31}\text{P}$  spectrum are very sharp (Figure 4B, left panel). This indicates that the DnaB:DNA complex fixes AMPPCP with high homogeneity.

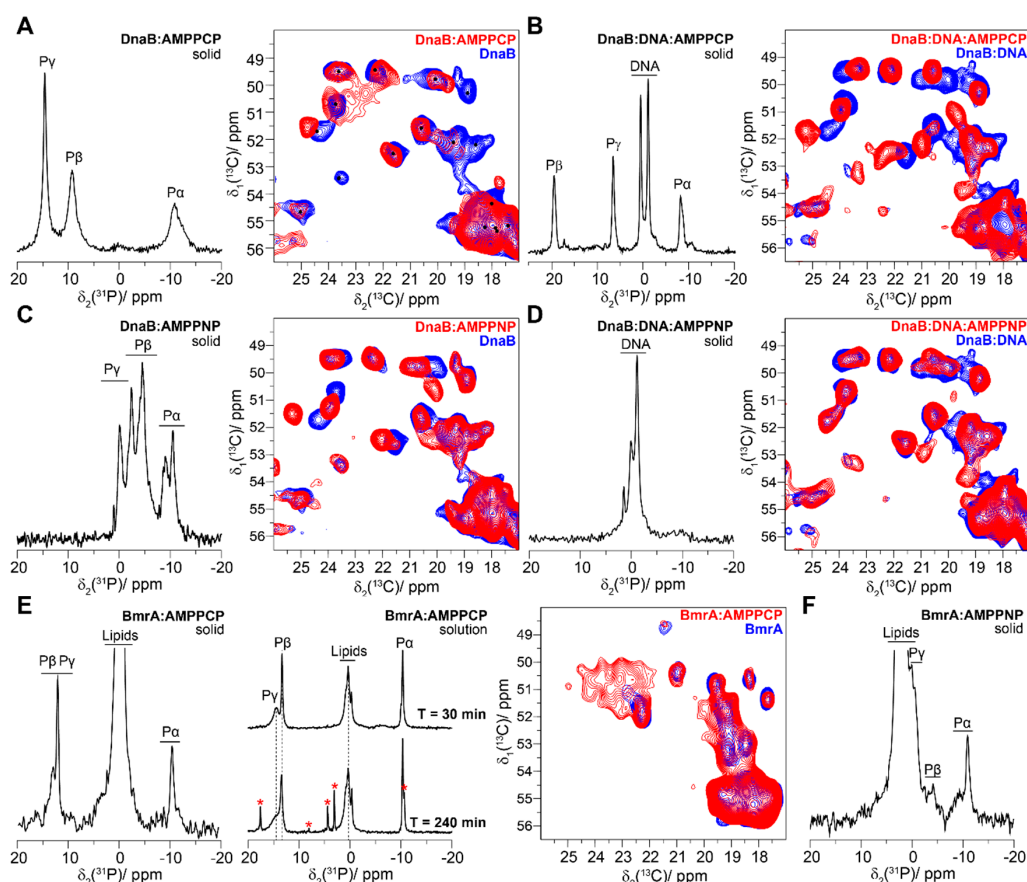


**Figure 4.** Pre-hydrolytic states using the systems DnaB and BmrA.  $^{31}\text{P}$  one dimensional spectrum cross-polarization (1D CP) spectrum (left panel) and the alanine region of  $^{13}\text{C}$ - $^{13}\text{C}$ -DARR spectra overlay (right panel) of DnaB (blue) and DnaB:AMPPCP (red) (A), DnaB:DNA (blue) and DnaB:DNA:AMPPCP (red) (B), DnaB (blue) and DnaB:AMPPNP (red) (C), DnaB:DNA (blue) and DnaB:DNA:AMPPNP (red) (D).  $^{31}\text{P}$  1D CP spectrum (left panel),  $^{31}\text{P}$  1D spectrum (middle panel) spectrum and overlay of the alanine region of  $^{13}\text{C}$ - $^{13}\text{C}$ -DARR spectra (right panel) of BmrA:AMPPCP (red) and BmrA (blue) (E). Red stars indicate hydrolysis products of AMPPCP.  $^{31}\text{P}$  1D CP spectrum of BmrA:AMPPNP (F). Spectra in (A) and (B) were adapted from Wiegand et al. 2019 [82] (<http://creativecommons.org/licenses/by/4.0/>), spectra (C) and (D) were adapted with permission from Wiegand et al. 2016 [38]. Panels (E) and (F) on BmrA represent original data; Red stars (\*) indicate hydrolysis products of AMPPCP.

The 2D  $^{13}\text{C}$ - $^{13}\text{C}$  DARR experiments recorded on DnaB:AMPPCP show not only chemical-shift perturbations when compared to the apo protein, but also dynamic changes, as can be seen in the extract of the alanine region (Figure 4A, right panel) by the disappearance of resonances, which could be assigned to the *N*-terminal domain [82], which is important for binding the DnaG primase within the primosome. As illustrated by the equivalent 2D  $^{13}\text{C}$ - $^{13}\text{C}$  DARR experiment on the DNA-bound DnaB (Figure 4B, right panel), the binding of AMPPCP induces stronger CSPs due to larger conformational changes of the protein, but no dynamic effects of the *N*-terminal domain were observed.

In principle, AMPPNP and AMPPCP should have a similar effect on DnaB, as both should induce the pre-hydrolytic state. However, it is clear from the NMR spectra that the effects of these two analogues are very different. First, as highlighted by the 1D CP  $^{31}\text{P}$  spectrum (Figure 4C, left panel), the presence of multiple resonances from the phosphate groups of AMPPNP indicates several structurally slightly different bound AMPPNP molecules. Interestingly, the 2D  $^{13}\text{C}$ - $^{13}\text{C}$  DARR spectrum reveals that the

disappearance of the *N*-terminal domain resonances upon binding of AMPPCP is not observed in case of AMPPNP (Figure 4C, right panel). Also, we had observed that in presence of DNA, all AMPPNP is hydrolysed by the helicase [38]. Consequently, as shown by Figure 4D right panel, no AMPPNP is bound to the protein when DNA binds to the helicase, and the 2D  $^{13}\text{C}$ - $^{13}\text{C}$  DARR spectrum of DnaB in the presence of AMPPNP looks highly similar to DnaB without the analogue, which is not detected in the  $^{31}\text{P}$  spectra either (Figure 4D left panel).

BmrA also binds AMPPCP, as shown by the 1D CP  $^{31}\text{P}$  spectrum (Figure 4E, left panel). However, the rate of AMPPCP hydrolysis is much higher, compared to DnaB, and degradation products of AMPPCP can be observed already four hours after the rotor filling in the supernatant of the NMR rotor, as shown in Figure 4E right panel (see red stars in the Figure). We recorded a 2D  $^{13}\text{C}$ - $^{13}\text{C}$  DARR experiment of BmrA:AMPPCP (two days of acquisition), and the spectrum is virtually the same as the one of BmrA in the apo state. Possibly, AMPPCP has been rapidly hydrolysed, and an insufficient amount of AMPPCP only remained bound on BmrA. Similar to AMPPCP, AMPPNP binds to BmrA (Figure 4F), but was also rapidly hydrolysed (data not shown). The analysis of  $^{31}\text{P}$  NMR spectra for protein samples containing lipids or DNA is more difficult due to the overlap between the  $^{31}\text{P}$   $\gamma$ - and  $\beta$ -phosphate signals from AMPPNP and those from lipid/DNA.

To overcome the hydrolysis problem with BmrA and to obtain a snapshot of the protein in its pre-hydrolytic state, we used an alternative approach, which is based on using mutant forms of the protein, which do bind ATP, but do not hydrolyse it. For this, catalytic residue/s can be mutated in order to make the protein inactive; still, one must take care that the protein retains its native fold. For BmrA, and also for other ABC transporters, it was shown that the mutation of the catalytic glutamate (E504 in BmrA) does not significantly affect the conformational change occurring upon nucleotide binding [23,99]. In contrast, the protein cannot achieve the pre-hydrolytic conformation when the nucleotide-binding Lys residue of the Walker A motif is mutated, here K380A [23,99]. We incubated the mutant E504A with ATP, and then sedimented it for analysis in the solid-state NMR rotor. While E504A is not completely inactive, it displays a very low ATPase activity (but still even crystals were obtained recently, PDB accession code 6R72, and a cryo-EM based structure was reported, PDB accession code 6R81) when compared to K380A, used as a fully inactive control (Figure 5A). After 40 h, only 50% of ATP is consumed, which allowed for the acquisition of 1D and 2D solid-state NMR experiments. The resulting 1D  $^{31}\text{P}$  CP spectrum displays three narrow peaks corresponding to the three phosphate groups from the ATP bound to the protein (Figure 5B). The 2D  $^{13}\text{C}$ - $^{13}\text{C}$  DARR spectrum displays CSPs and peaks appearing, both induced by the conformational and dynamic changes in the protein as a consequence of ATP binding (Figure 5C) [92].

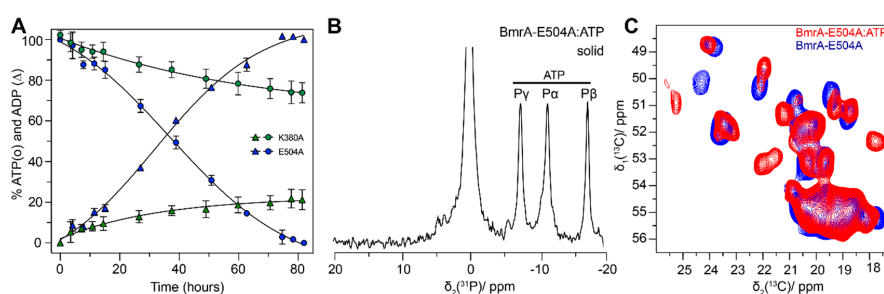


**Figure 5.** Pre-hydrolytic states using the system BmrA-E504A (catalytically inhibited). Percentage of ADP ( $\Delta$ ) and ATP ( $\circ$ ) in the presence of the mutant BmrA-E504A (symbol filled in blue) or of the mutant, which does not bind the nucleotide, BmrA-K380A (symbol filled in green). BmrA-K380A was chosen as a negative control in order to exclude the possibility of an ATPase contaminant in the sample (A).  $^{31}\text{P}$  1D CP spectrum of BmrA-E504A:ATP (B). The overlay of the alanine region of  $^{13}\text{C}$ - $^{13}\text{C}$ -DARR spectra of BmrA-E504A (blue) and BmrA-E504A:ATP (red) (C). Results in panels (A) and (B) are original, and spectra in (C) were adapted from Lacabanne et al. 2019 [92] (<http://creativecommons.org/licenses/by/4.0/>).

To summarize, our data show that analysis of the pre-hydrolytic state is difficult both for DnaB and BmrA, since first the corresponding ATP mimics do not behave in a homogenous manner, i.e., analogues which should yield similar states lead to different NMR spectra, and second, most popular analogues are actually hydrolysed by the helicase in presence of DNA, as well as by the ABC transporter.

With respect to the first point, the intriguing observation that the AMPPCP- and AMPPNP-induced pre-hydrolytic states show conformational differences might be linked to the proposition that one can further differentiate each pre-hydrolytic mimic, as discussed by Ogawa et al., and assign the different mimics to specific steps therein: ATP- $\gamma$ -S for the initial pre-hydrolysis state, AMPPCP for the pre-isomerization state, ADP:BeF<sub>x</sub> for the middle pre-hydrolysis state and AMPPNP for the late pre-hydrolysis state [107]. It is difficult to establish a similar statement for DnaB, as one can also explain these differences by the fact that these analogues can behave differently from ATP in terms of their chemical properties: as examples for AMPPNP the oxygen, a hydrogen bond acceptor, is replaced by an NH<sub>2</sub> group, a possible hydrogen bond donor; AMPPCP has one oxygen atom less than ATP.

With respect to the second point, in the DnaB-DNA complex, only AMPPCP resisted to hydrolysis, and was the best choice to study DnaB and its DNA complex. It was however, rapidly hydrolysed in BmrA, which might be caused by the very high ATPase activity of BmrA, which is with an activity of 6.5  $\mu\text{mol}\cdot\text{min}^{-1}\cdot\text{mg}^{-1}$  one of the most active ABC transporters (one to three orders of magnitude higher than typical ABC transporters) [108]. Amongst AMPPNP and ATP- $\gamma$ -S, which are the most used pre-hydrolytic state analogues for ABC transporters and helicases (see Figure 3B), neither proved useful here. Alternative strategies using mutant forms were successful to analyse a pre-hydrolytic mimic of the protein and presents a valuable alternative when ATP analogues fail to mimic the pre-hydrolysis states.

#### 4.2. The Transition-State Analogues ATP/ADP:Vi and Aluminium Fluorides (ADP:AlF<sub>x</sub>)

In order to investigate the transition states of BmrA and DnaB, we used the solid-state NMR techniques already described above, and also complemented them by EPR (Figure 1). The conformation of DnaB in the presence of ADP:Vi was compared with DnaB apo (Figure 6A) and DnaB in the presence of ADP only (Figure 6B). We also studied the protein with ADP and DNA, in the presence or absence of vanadate (Figure 6C).

The <sup>13</sup>C-<sup>13</sup>C 2D DARR spectra of DnaB apo and DnaB:ADP:Vi display a few shifting resonances upon binding of the nucleotide (Figure 6A). However, the comparison of DnaB:ADP with and without vanadate shows that the NMR fingerprints of both samples are actually highly similar (Figure 6B), indicating that vanadate did not bind to the NBD and did not induce significant conformational changes. In contrast, when DNA is added to both samples, the NMR spectra of DnaB:ADP:Vi+DNA are different from the ones in the absence of DNA (DnaB:ADP:Vi and DnaB:ADP), with significant CSPs, but the most obvious CSPs are observed for the complex DnaB:ADP:DNA (Figure 6C, left panel). Since these two samples behave differently, a <sup>31</sup>P NMR spectrum was recorded to probe the bound ATP-mimics. The 1D <sup>31</sup>P-CP spectrum of DnaB:ADP:DNA displays two phosphorus peaks assigned to DNA (two DNA nucleotides bind to one DnaB monomer leading to two different phosphate binding environments [82]), and four peaks which can be assigned to bound ADP [88] (Figure 6C, right panel). P $\alpha$  and P $\beta$  correspond to the DnaB:ADP complex in the absence of DNA, and P $\alpha'$  and P $\beta'$  to the DnaB:ADP:DNA complex, indicating an insufficient DNA concentration to saturate the protein completely with DNA. However, the 1D <sup>31</sup>P-CP spectrum of DnaB:ADP:Vi:DNA (Figure 6C, right panel) shows only one population of ADP, with <sup>31</sup>P chemical-shift values similar to the DnaB:ADP complex, and a reduced intensity of the peaks assigned to the DNA. One can conclude from these spectra that the presence of vanadate actually inhibits the binding of DNA to DnaB.

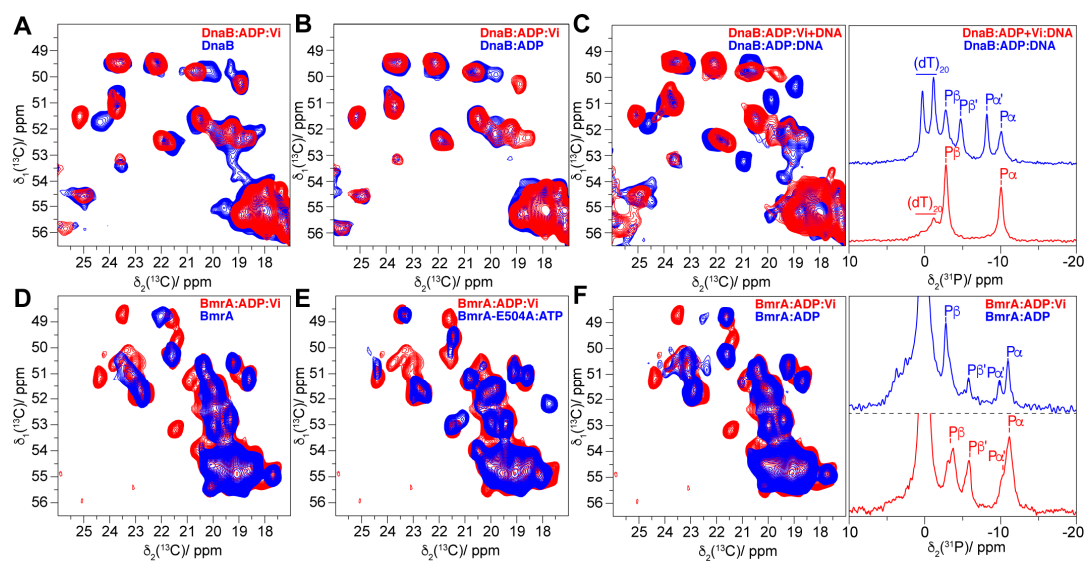


**Figure 6.** Comparison of the effect of vanadate on BmrA and DnaB. Alanine region from  $^{13}\text{C}$ - $^{13}\text{C}$ -DARR spectra of DnaB:ADP:Vi overlaid with DnaB apo (A), DnaB:ADP (B). Alanine region from  $^{13}\text{C}$ - $^{13}\text{C}$ -DARR (C, left panel) and 1D  $^{31}\text{P}$ -CP (C, right panel) spectra of DnaB:ADP:Vi;DNA overlaid with DnaB:ADP:DNA. Alanine region from  $^{13}\text{C}$ - $^{13}\text{C}$ -DARR spectra of BmrA:ADP:Vi overlaid with BmrA apo (D), BmrA-E504A:ATP (E) and BmrA:ADP (left panel) complemented with the 1D  $^{31}\text{P}$  spectrum (F, right panel). The resonance peak from the lipids (0 ppm) was cut, the separation between the two spectra is indicated by a dashed line. The blue spectrum in (A) was adapted from Wiegand et al. 2019 and spectra (D) and (E) were adapted from Lacabanne et al. 2019 [82,92] (<http://creativecommons.org/licenses/by/4.0/>). The red spectra in (A) and (C), as well as the spectra in (F) are original data.

For the ABC transporter BmrA, one must say beforehand that conformational changes are not observed in BmrA upon incubating with vanadate and ADP. The protein requires vanadate and ATP instead of ADP, since ATP hydrolysis is required to induce the conformational changes. The inorganic phosphate is then exchanged by a vanadate anion, and Vi and ADP remain bound. The comparison between the  $^{13}\text{C}$ - $^{13}\text{C}$  DARR spectra of BmrA apo and BmrA:ATP:Vi shows both CSPs and new appearing peaks (Figure 6D). The presence of additional signals appearing in the protein spectra is indicative of a decrease of the flexibility of the corresponding protein residues [92]. When compared to the pre-hydrolytic state (obtained with BmrA-E504A:ATP), the new peaks appearing in the spectra overlay to a large extent (Figure 6E), indicating that these residues show a similar conformation. Some differences with respect to the pre-hydrolytic state can be observed, which can be associated to the addition of vanadate. To highlight the effect of vanadate, the spectrum of BmrA:ADP:Vi was compared to BmrA:ADP only (Figure 6F). This revealed the presence of new peaks, but only minor CSPs. The appearing peaks can serve as the fingerprint pattern that allows to distinguish the pre-hydrolytic and transition states, while the CSPs serve as the fingerprint pattern reflecting the kind of nucleotide bound.

A 1D  $^{31}\text{P}$ -CP NMR experiment can yield complementary information about the bound ATP-mimics (Figure 6F, right panel). The  $^{31}\text{P}$  spectrum of BmrA:ADP shows the presence of two populations of ADP (labeled  $\text{P}\alpha$ ,  $\text{P}\beta$  and  $\text{P}\alpha'$ ,  $\text{P}\beta'$ ), and the presence of vanadate induces  $^{31}\text{P}$  chemical-shift changes for BmrA which were not observed for DnaB [12]. In case of BmrA:ADP:Vi, two populations of  $\text{P}\beta$  can be clearly distinguished and also for  $\text{P}\alpha$ , but less significantly ( $\text{P}\beta$  of ADP with vanadate has a different chemical shift than  $\text{P}\beta$  of ADP without vanadate). It is known that the trapping of one nucleotide during the transition state (in presence of vanadate) is possible while the second nucleotide can be poorly bound. This property has been observed for several ABC transporters (p-gp [109]; BmrA [99]; LmrA [110]; Maltose transporter [53]) suggesting an asymmetry of the NBDs [111].

In order to gain additional insight into whether vanadate binding occurred or not, we performed EDNMR experiments. This approach can be used to detect the  $^{51}\text{V}$  nucleus ( $I = 7/2$ ) in proteins in which the  $\text{Mg}^{2+}$  has been replaced by the EPR-active  $\text{Mn}^{2+}$  metal ion [16,112] in the nucleotide-binding sites, as sketched in Figure 1. The experiment detects the hyperfine couplings of the unpaired electrons of  $\text{Mn}^{2+}$  to the nuclei in the vicinity. We applied this both to the ABC transporter and the DnaB helicase. One should mention that it was shown by biochemical investigations for both proteins that upon substitution of  $\text{Mg}^{2+}$  by  $\text{Mn}^{2+}$ , their biological function is maintained [86,113]. Figure 7 shows the resulting EDNMR spectrum for the BmrA:ADP:Vi complex (shown in red) with an intense resonance for  $^{51}\text{V}$  (for the echo-detected field-swept EPR spectra see Figure S2). In the absence of protein in the sample (black line) the spectrum only shows a  $^{51}\text{V}$  peak with very low intensity assigned to vanadate in solution. Unresolved couplings to  $^{23}\text{Na}$  would appear at very similar frequencies. We thus conclude that vanadate binds to the NBD in the case of BmrA.

For DnaB, no  $^{51}\text{V}$  peak can be observed in the EDNMR spectrum, indicating that no vanadate is found in the vicinity of  $\text{Mn}^{2+}$  (Figure 7B). The EDNMR spectrum indeed shows the same profile for DnaB in the presence of nucleotide with vanadate (red line) and without (black line). We can thus exclude the presence of vanadate in the NBD of the protein. However, as shown previously in Figure 6B, some spectral differences (mainly appearing peaks upon ADP:Vi incubation) can be noticed when DnaB:ADP:Vi was compared to DnaB:ADP. In other words, these experiments do not allow to exclude that vanadate might bind at another location than in the NBD.

We thus used a complementary experiment which can directly detect  $^{51}\text{V}$  using solid-state NMR.  $^{51}\text{V}$  has been intensively studied by solid-state NMR due to its rather small nuclear quadrupole moment and its high sensitivity [114–116]. Vanadate has also been studied in biological systems using solution-state NMR [117,118] and solid-state NMR [119]. Figure 7C shows the  $^{51}\text{V}$  MAS spectrum of DnaB:ADP:Vi recorded at two different MAS spinning frequencies of 17 and 19 kHz. By measuring at two different MAS frequencies, the central transition ( $| -1/2 \rangle \leftrightarrow | +1/2 \rangle$ , to first order free from quadrupole interaction, can be distinguished from the spinning-sideband positions resulting from first-order quadrupolar interaction (a superposition of the remaining single-quantum transitions, marked by asterisks). The presence of the first order quadrupolar coupling sideband pattern already points to immobilized  $^{51}\text{V}$  species. We can distinguish two resonances at around  $-600$  ppm ( $-604$  ppm and  $-618$  ppm) and two further vanadate species bound to DnaB at  $-533$  and  $-681$  ppm (Figure 7C). To assign those resonances, a spectrum of the not immobilized (the supernatant)  $^{51}\text{V}$  was recorded and assigned (Figure 7D). The resonances of the  $^{51}\text{V}$  MAS spectrum can be assigned by comparison with the solution-state spectrum of the supernatant as follows:  $\text{VO}_4^{3-}$  (V1),  $\text{V}_2\text{O}_7^{4-}$  (V2),  $\text{V}_4\text{O}_{12}^{4-}$  (V4) and  $\text{V}_5\text{O}_{15}^{5-}$  (V5) [120,121]. We can exclude that the peaks corresponding to the immobilized phase peaks result from the precipitation of vanadate, since with an initial orthovanadate concentration of  $5$  mM ( $0.92$  g  $\text{L}^{-1}$ ) at pH 6, we are two orders of magnitude below the solubility limit. The detected signal thus must stem from DnaB-bound vanadate, which might be related to the observation that addition of vanadate interferes with DNA binding to DnaB (Figure 6C).

To sum up, vanadate is a reasonable ATP-transition-state mimic for the ABC transporter BmrA. The transporter is trapped, most likely in its outward-facing state, when binding ADP:Vi. The transition state is characterized by a characteristic fingerprint in the NMR  $^{13}\text{C}$ - $^{13}\text{C}$  DARR spectrum, and vanadate is indeed present in the vicinity of the metal ion. In contrast, ADP:Vi is not a suitable ATP-transition-state mimic for the helicase DnaB. Indeed, solid-state NMR and EPR experiments reveal that vanadate does not bind to the NBD together with the nucleotide. Instead, vanadate is bound elsewhere to DnaB, most likely in an unspecific manner. ADP:Vi strongly inhibits binding of DNA, suggesting that they share the same binding site on DnaB, and that vanadate outcompetes DNA.

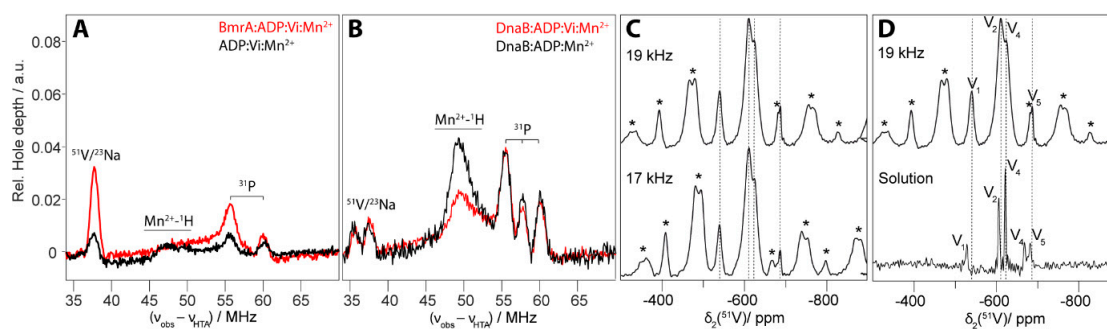


**Figure 7.** Localisation of the vanadate ion using NMR and EPR experiments. Background corrected 94 GHz EDNMR spectra of BmrA (A) and DnaB (B) incubated with  $Mn^{2+}$  and ADP, with and without vanadate. For  $^{31}P$ , a doublet due to the hyperfine coupling to  $^{31}P$  is observed ( $\sim 4$  MHz), as well as a singlet not assigned so far [122].  $^{51}V$  spectra of DnaB:ADPMg:DNA:Vi recorded at a MAS frequency of 17 and 19 kHz (C).  $^{51}V$  spectra of DnaB:ADPMg:DNA:Vi overlaid with the solution-state spectrum of ADPMg:Vi (D). Central transitions are indicated with dashed lines whereas spinning sidebands are indicated with a black star. All panels represent original data.

#### 4.3. Aluminium Fluorides ( $AlF_x$ ) as Transition-State Mimic

$AlF_x$  is the most frequently used transition-state analogue (Figure 2A), although the pH-dependence of its formation imposes certain limitations to it. At  $pH \geq 5$  (depending also on the concentration and the anions in the solution),  $Al^{3+}$  starts to form an aluminium hydroxide complex,  $Al(OH)_3$ , which is insoluble. However, the presence of an excess of fluoride shifts the pH upon which  $Al(OH)_3$  formation occurs to a higher value. We calculated the concentrations of the different species of aluminium under the conditions used (6 mM of  $AlCl_3$  and 30 mM  $NH_4F$ ) as a function of the pH-value (Figure 8). In our case, the formation of  $Al(OH)_3$  starts at pH 7, and almost all  $Al^{3+}$  precipitates as  $Al(OH)_3$  at  $pH \geq 8$ . The amount of formed  $AlF_x$  is thus not sufficient to induce the protein: $AlF_x$  complex formation. At the same time, fluorides present in the solution can form a complex with  $Mg^{2+}$  generating the transition-state analogue  $MgF_3^-$ . This effect was followed and confirmed by  $^{19}F$  NMR for the conversion of a protein:ADP: $AlF_4^-$  complex to a protein:ADP: $MgF_3^-$  complex by increasing the pH [56]. Moreover, as pointed out above,  $MgF_3^-$  and  $AlF_3$  are structurally very similar and some structures comprising  $AlF_3$  as transition state mimic are in reality  $MgF_3^-$  because they were obtained at  $pH \geq 8$  [56–58].

For DnaB, the DnaB:ADP: $AlF_x$  complex can easily be prepared at a pH of 6, since the protein is stable at this pH value. In the presence of the transition-state analogue, the 1D CP  $^{31}P$  spectrum displays two very narrow resonances assigned to the  $P\alpha$  and  $P\beta$  of ADP in complex with  $AlF_x$  (Figure 9A, left panel). Note a minor amount of DnaB:ADP in the sample. The 2D  $^{13}C$ - $^{13}C$  DARR spectrum of DnaB:ADP: $AlF_x$  displays strong CSPs attributed to conformational changes of the protein (Figure 9A, right panel). While we noticed that the use of vanadate inhibits the binding of DNA, DNA clearly binds to DnaB in the presence of  $AlF_x$ , as shown by Figure 9B, left panel. Fluorescence anisotropy measurements revealed that the affinity for DNA-binding is even the highest in the presence of ADP: $AlF_x$  compared to the other ATP-mimics used [82]. The 2D  $^{13}C$ - $^{13}C$  DARR spectrum of the sample in presence of DNA reveals that several peaks, which belong to the N-terminal domain, are again missing, indicating a change in the dynamics of the protein, as was already observed for DnaB:AMPPCP without DNA.

The case of BmrA is more complex, since the optimal pH for sample preparation lies at 8. For optimal use of  $AlF_x$ , the pH would need to be lowered, but we observed this to result in poor (e.g., strongly broadened) spectra. Nevertheless, we explored this further, and in order to test the pH dependency, BmrA, in the presence of ATP, was incubated with 6 mM of  $AlCl_3$  and 30 mM  $NH_4F$  at pH 8, 7.5 and 7, and a 1D CP  $^{31}P$  NMR was recorded for all three conditions (Figure 9C, left panel). The 1D CP  $^{31}P$  NMR spectrum at pH 8 shows that ATP/ADP is abundantly co-precipitated with  $Al(OH)_3$  which makes the 1D spectrum difficult to analyse due to a broad and rather unstructured resonance of this amorphous species (Figure 9C, left panel). As expected, the fraction of ATP/ADP co-precipitated

with  $\text{Al}(\text{OH})_3$  decreases with decreasing pH-values. While at pH 7 the precipitation of  $\text{Al}(\text{OH})_3$  is still visible in the  $^{31}\text{P}$  NMR spectrum, one can compare it to  $\text{BmrA}:\text{ADP}:\text{Vi}$ , which shows that both spectra overlay with only few minor differences (Figure 9D, right panel). This indicates that the conformation is highly similar to the one observed with vanadate. A 2D  $^{13}\text{C}$ - $^{13}\text{C}$  DARR spectrum recorded on the pH 7 sample (Figure 9C, right panel) confirms this, as the resonances largely superimpose.

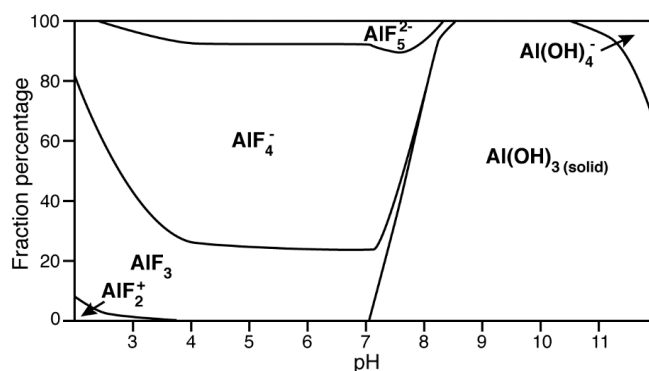


**Figure 8.** The different species of  $\text{AlF}_x$  at different pH. The diagram was generated using ChemEQL [123], which calculates chemical speciation and equilibria. Concentrations used were 6 mM  $\text{AlCl}_3$  and 30 mM  $\text{NH}_4\text{F}$ .

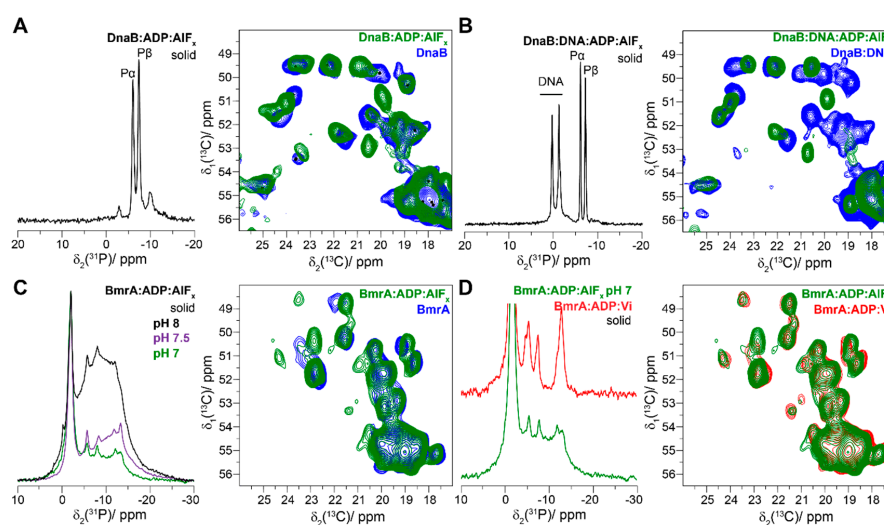


**Figure 9.** Comparison of the metal fluoride  $\text{AlF}_x$  on the systems  $\text{BmrA}$  and  $\text{DnaB}$ . 1D CP of  $\text{BmrA}:\text{ADP}:\text{AlF}_x$  at different pH (A, right panel) and  $^{13}\text{C}$ - $^{13}\text{C}$ -DARR spectra of the alanine region of  $\text{BmrA}:\text{ADP}:\text{AlF}_x^-$  (green) and  $\text{BmrA}$  (A, left panel, blue).  $^{31}\text{P}$  1D CP spectra of  $\text{BmrA}:\text{ADP}:\text{AlF}_x$  at pH 7 overlaid with  $\text{BmrA}:\text{ADP}:\text{Vi}$  (B, right panel) and  $^{13}\text{C}$ - $^{13}\text{C}$ -DARR spectra of the alanine region of  $\text{BmrA}:\text{ADP}:\text{AlF}_x$  and  $\text{BmrA}:\text{ADP}:\text{Vi}$  (B, left panel).  $^{31}\text{P}$  1D CP spectrum (left panel) and  $^{13}\text{C}$ - $^{13}\text{C}$ -DARR the alanine region spectra overlay (right panel) of  $\text{DnaB}$  and  $\text{DnaB}:\text{ADP}:\text{AlF}_x$  (C),  $\text{DnaB}:\text{DNA}$  and  $\text{DnaB}:\text{DNA}:\text{ADP}:\text{AlF}_x$  (D). Spectra (A) and (B) were adapted from Wiegand et al. 2019 [82] (<http://creativecommons.org/licenses/by/4.0/>). Panels (C) and (D) present original data.

To summarize, the use of  $\text{AlF}_x$  as a transition analogue heavily depends on the optimal pH value of the protein. Indeed, biological systems are principally studied at pH 5–9, and it is important to take into account the formation and precipitation of  $\text{Al}(\text{OH})_3$  at pH  $\geq 7$  under our conditions. The spectra of  $\text{BmrA}$  at pH  $\geq 7$  well illustrate the consequences of the use of  $\text{AlF}_x$  in alkaline conditions. The protein actually adopts a similar conformation as in the presence of vanadate, but high amounts of amorphous

species are detected. In contrast, DnaB at pH 6 shows high affinity to  $AlF_x$  which induces substantial conformational changes; and also DNA binding is not affected.

#### 4.4. The Post-Hydrolytic State Induced by ADP

The last state in the ATP hydrolysis cycle is the post-hydrolytic state, where ADP is still bound to the protein and the inorganic phosphate (previously  $\gamma$ -phosphate) is released from the binding pocket. This state is well mimicked by the addition of ADP. We used the  $^{31}P$  and  $^{13}C$  experiments described above to characterize BmrA and DnaB in the presence of ADP.

The  $^{31}P$  CP spectrum for DnaB:ADP is shown in Figure 10A (left panel). The spectrum displays two sharp peaks, which indicates a good homogeneity of the sample. The overlay of the 2D DARR spectra DnaB:ADP and DnaB apo (Figure 10A, right panel) reveals CSPs and also the disappearance of *N*-terminal domain peaks, indicating conformational changes and an increase in the dynamics of the protein.

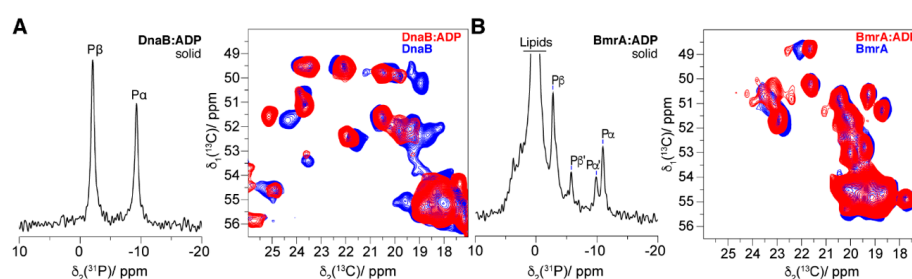


**Figure 10.** Generation of the post-hydrolytic state using ADP. (A)  $^{31}P$  1D CP spectrum (left panel) and  $^{13}C$ - $^{13}C$ -DARR the alanine region spectra overlay (right panel) of DnaB:ADP/DnaB apo; (B)  $^{31}P$  1D CP spectrum (left panel) and  $^{13}C$ - $^{13}C$ -DARR the alanine region spectra overlay (right panel) of BmrA:ADP/BmrA. Spectra (A) were adapted from Wiegand et al. 2019 [82] (<http://creativecommons.org/licenses/by/4.0/>), and spectra in panel (B) are original data.

In contrast, the conformational changes of the ABC transporter BmrA are minor between the presence and absence of ADP. First of all, the  $^{31}P$  CP spectrum shows the presence of two populations of ADP as identified by peak doubling, labeled  $P\alpha$ ,  $P\beta$ , and  $P\alpha'$ ,  $P\beta'$  (Figure 10B, left panel). These two populations are the result of two different binding modes of ADP to the protein. However, since the intensity of the  $P\alpha'$ ,  $P\beta'$  peaks is 50% lower than  $P\beta$ ,  $P\alpha$ , there is less  $P\alpha'$ ,  $P\beta'$  bound to the protein than  $P\beta$ ,  $P\alpha$ . This is reminiscent to the pattern that was observed with vanadate (Figure 6F). Unspecific binding of ADP to the protein can explain this observation. Secondly, the overlay of the 2D DARR spectra of BmrA:ADP and BmrA apo displays few CSPs compared to what we observed in the presence of other ATP analogues. In contrast to DnaB, the binding of ADP does not induce large conformational or dynamics changes in the protein, and binding of ADP to BmrA seems to be very weak.

#### 4.5. Structural Considerations

It seems worthy to compare the NMR data with structural information as available for proteins that are closely related to DnaB of *Helicobacter pylori* and BmrA of *Bacillus subtilis*, respectively.

*BmrA and its structural counterpart.* The most suited for comparison appears to be the set of structures that shows the maltose ABC-transporter of *E. coli* (MBP-MalFGK2) in the outward-facing conformation, with two interacting NBDs and in the presence of AMPPNP (PDB 3RLF), ADP:BeF<sub>3</sub> (PDB 3PUX), ADP:Vi (PDB 3PUV), and ADP:AlF<sub>4</sub><sup>-</sup> (PDB 3PUW) [64]. The collection of these different structures shapes the view of the transport cycle [122]. Chen and Oldham noticed that, despite the different ATP-analogues used, all residues within the NBD are essentially superimposable. However, structural differences between the pre-hydrolytic state (AMPPNP) and the transition state (ADP:Vi and ADP:AlF<sub>4</sub><sup>-</sup>) are (i) the distance between the  $\gamma$ -phosphate or the mimicked  $\gamma$ -phosphate by the analogues and the bridging oxygen of

the  $\beta$ -phosphate and (ii) the presence of a water molecule, essential for the ATP hydrolysis, only in the transition state. Although the transmembrane part of the maltose transporter essentially differs from that of BmrA, the NBD homodimers of the two proteins are relatively similar (RMSD of 1.7 Å from the alignment of MBP-MalFGK2:AMPPNP, PDB 3RLF, with BmrAE504A:ATP, PDB 6R72). The two NBDs differ mainly in their ATPase activity. The ATPase activity of MBP-MalFGK2 is one order of magnitude lower than BmrA [124]. For BmrA, a major conformational transition between the open (inward-facing) and closed (outward-facing) conformation was for example experimentally demonstrated by hydrogen/deuterium exchange (HDX) coupled to mass spectrometry [125] and NMR spectroscopy [92]. It is believed that the protein adopts the closed conformation, with interacting NBDs, upon substrate binding. Generally, in membrane transporters, the energies of their sub-conformations should be close to each other and should essentially depend on the protein environment. The NMR spectra of BmrA in the presence of ADP:Vi and ADP:AlF<sub>4</sub><sup>-</sup> might be taken as reporters of the enzyme transition state; in the presence of AlF<sub>4</sub><sup>-</sup>, the crystal structure of the maltose transporter shows a classical picture with the catalytic water molecule in the apical attack position (Figure 11A). Even in the presence of AlF<sub>4</sub><sup>-</sup>, the <sup>31</sup>P 1D CP spectra give two signals for the  $\alpha$ - and  $\beta$ -phosphates (Figure 9D), respectively, which points to a certain nonequivalence of the two substrate-binding sites in the two similar NBDs. This finding might indicate that the two catalytic sites operate not simultaneously but sequentially.

*DnaB of Helicobacter pylori and its structural counterparts.* The conformation of DnaB, as could be judged from the 2D <sup>13</sup>C-<sup>13</sup>C DARR spectra, essentially depends on the nature of the analogue used, which matches the great structural variability reported for DnaB from other bacteria and their viral homologues [126–132]. Depending on the presence of substrate analogues and their nature, the SF4 helicase subunits can either form rings of distinct shapes [126–130] or arrange themselves as a hexameric ladder along a DNA strand [131,132]. The latter type of the structure was reported for DnaB from *Bacillus stearothermophilus* (currently *Geobacillus stearothermophilus*), which was crystallized, in the presence of a DNA strand, with GDP:AlF<sub>4</sub><sup>-</sup> in five of its six catalytic sites [131] (see Figure 11B). In this structure, each monomer of DnaB interacts in a similar way with two nucleotides of DNA; together, the subunits make a kind of a spiral ladder. It is noteworthy, that the position of AlF<sub>4</sub><sup>-</sup> in the structure of *Geobacillus stearothermophilus* DnaB (Figure 11B) differs from that in other P-loop fold NTPases. No catalytic water molecule is present apically to the plane of AlF<sub>4</sub><sup>-</sup> (see Figure 11A as a typical example), and the position of the AlF<sub>4</sub><sup>-</sup> moiety does not correspond to that of the  $\gamma$ -phosphate group (see Figure 11C,F). Interestingly, the NMR data on DnaB from *Helicobacter pylori* discussed herein point to a full occupation of all six NBDs and a rather high symmetry in the oligomer [82] as it potentially could be achieved by more flat conformations of the helicase hexamer, as reported for several DnaB proteins, including the one from *Geobacillus stearothermophilus*, which were crystallized in the absence of AlF<sub>4</sub><sup>-</sup> [127,128]. Whether the physiological shape of the DnaB ring is flat or spiral has to be established yet.

Figure 11D,E show the structures of the NBD of the ABC transporter MBP-MalFGK2 (Figure 11D) and the gene 4 helicase from bacteriophage T (Figure 11E) complexed with the pre-hydrolytic ATP analogue AMPPNP. The overlay of the structures (Figure 11F) shows a similar conformation of the bound phosphate chain of the ATP mimic. Although quite similar enzymes seem to bind ATP mimics in a similar way, they might behave differently to the huge number of ATP analogues available and solid-state NMR seems to be the method-of-choice to address such different behaviors.

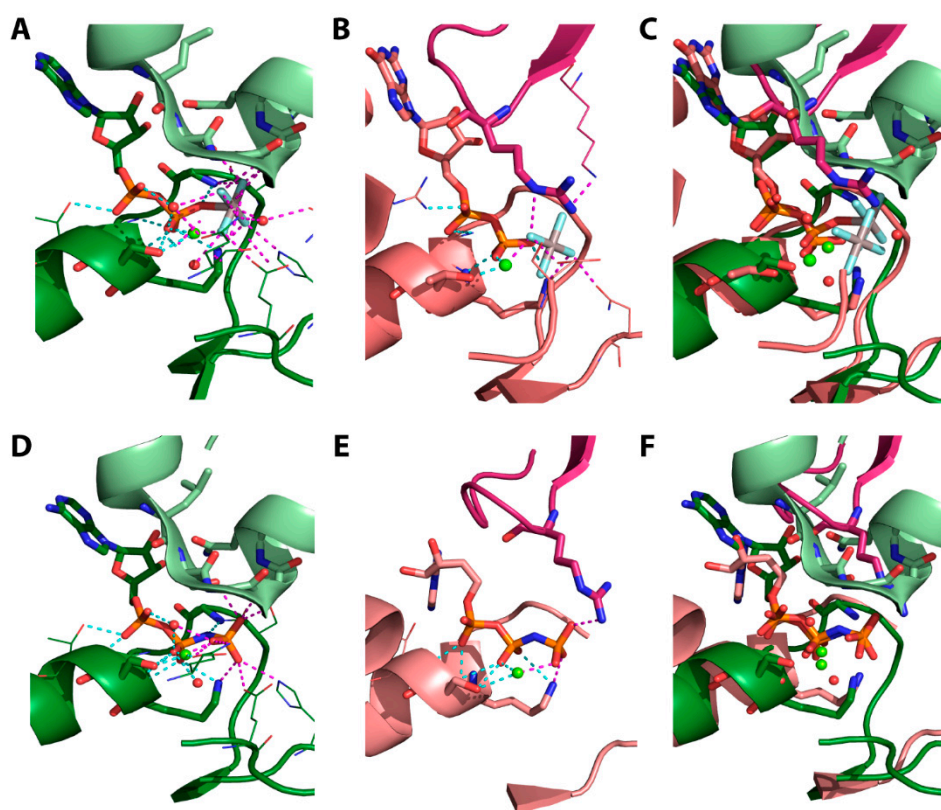


**Figure 11.** Structural comparison of nucleotide-binding sites in SF4 helicases and ABC-transporters. Different protein subunits are colored in different shades of the same color.  $Mg^{2+}$  or  $Ca^{2+}$  ions are shown as green spheres; water molecules are shown as red spheres; hydrogen bonds and metal interactions involving  $\alpha$ - and  $\beta$ -phosphates are shown as cyan dashes, interactions with  $\gamma$ -phosphate or its fluoroaluminate complex mimic shown as magenta dashes. Nucleotide analogue, P-loop motif residues and activating residues (Arg residue or LSGGQ motif) are shown as thick sticks, other interacting amino acid residues are shown as thin sticks. Enzymes complexed with  $NDP:AlF_4^-$  (A–C). Maltose/maltodextrin import ATP-binding protein MalK from *Escherichia coli* K-12 (PDB ID 3PUW, chain B) (A), Replicative helicase DnaB from *Geobacillus stearothermophilus* (PDB ID 4ESV, chain E) (B), Structures 4ESV and 3PUW superimposed by phosphate chain and ribose atoms of NDP moieties (C); Enzymes complexed with the slowly hydrolyzable ATP analogue AMPPNP (D–F). Maltose/maltodextrin import ATP-binding protein MalK from *Escherichia coli* K-12, (PDB ID 3RLF, chain A) (D), Gene 4 Ring Helicase from *Escherichia* phage T7 (PDB ID 1E0J, chain A) (E), Structures 1E0J and 3RLF superimposed by phosphate chain (F).

## 5. Conclusions

We herein reviewed magnetic-resonance approaches (in combination with additional data) to provide information at the atomic level on the binding of mimics of the different ATP forms present during the hydrolysis cycle. We investigated this for two ATP-fuelled proteins, an ABC transporter and a DNA helicase (Table 2), both driven by an ATPase motor domain. We showed that the ATP analogues mainly used for structural studies for such systems, AMPPNP and ATP- $\gamma$ -S, are not suitable for the systems studied here, since both are hydrolysed by the proteins. Furthermore, we show that analogues which should induce the same state in the hydrolysis cycle can fail to do so, since they result in different conformations. We also discuss that some analogues can interfere with protein function, such as DNA binding for DnaB. NMR, and also EPR, are sensitive tools to assess the impact of different analogues for a given protein, a need that arises through the observation that they can have widely differing effects on different proteins. NMR spectroscopy could be of help in tracing minor differences both in the overall protein conformation and in the state of the phosphate groups. Here we showed

that solid-state NMR enabled revealing notable differences in the structural properties of closely related P-loop fold NTPases, namely the SF4 DnaB helicase and BmrA ABC-transporter, which both belong to the same division of ASCE-NTPases.

**Table 2.** Summary of the ATP analogue efficiencies for the two protein systems BmrA and DnaB. ++ indicates high efficiency, + moderate efficiency, - low efficiency and – not efficient.

Analogue	State Being Mimicked	Suitability		Comments
		DnaB	BmrA	
AMPPNP	Pre-hydrolytic	-	-	Hydrolysed by DnaB in the presence of DNA Hydrolysed by BmrA
AMPPCP	Pre-hydrolytic	++	-	Rigidifies DnaB in the presence of DNA Hydrolysis observed
ATP- $\gamma$ -S	Pre-hydrolytic	-	-	Hydrolysed by BmrA and DnaB
V <sub>i</sub>	Transition-state	-	++	Inhibits the DNA binding in DnaB Provides the transition state for BmrA
AIF <sub>x</sub>	Transition-state	++	+	Provides the transition state for DnaB and BmrA Starts to precipitate at pH $\geq$ 7
ADP	Post-hydrolytic	++	++	Provides the post-hydrolysis state in both systems

**Supplementary Materials:** The following are available online [133–137].

**Author Contributions:** D.L. and R.C. prepared the samples. D.L. and T.W. performed the NMR experiments. N.W. and D.K. recorded the EPR experiments. M.I.K. and A.Y.M. analysed the protein structures. D.L., T.W., M.I.K., N.W., D.K., A.Y.M., B.H.M. and A.B. analysed the data. All authors contributed to the writing of the manuscript. D.L., T.W., B.H.M. and A.B. designed the research, and B.H.M. and A.B. supervised the project. All authors have read and agreed to the published version of the manuscript.

**Funding:** This work was supported by the ETH Career SEED-69 16-1 (T.W.) and the ETH Research Grant ETH-43 17-2 (T.W.), an ERC Advanced Grant (B.H.M., grant number 741863, FASTER), by the Swiss National Science Foundation (B.H.M., grant number 200020\_159707 and 200020-188711), the French Agence Nationale de Recherche (A.B., ANR-14-CE09-0024B, ANR-19-CE11-0023), the LABEX ECOFECT (A.B., ANR-11-LABX-0048) within the Université de Lyon program Investissements d’Avenir (A.B., ANR-11-IDEX-0007), the EvoCell Program of the Osnabrueck University (M.I.K.) and a grant from the Russian Science Foundation (A.Y.M., 17-14-01314).

**Acknowledgments:** We thank Gunnar Jeschke for his comments on the manuscript. D.L. and T.W. acknowledge helpful discussion with Marco E. Weber.

**Conflicts of Interest:** The authors declare no conflict of interest.

## References

- Manna, R.N.; Dutta, M.; Jana, B. Mechanistic study of the ATP hydrolysis reaction in dynein motor protein. *Phys. Chem. Chem. Phys.* **2020**, *22*, 1534–1542. [[CrossRef](#)] [[PubMed](#)]
- Mächtel, R.; Narducci, A.; Griffith, D.A.; Cordes, T.; Orelle, C. An integrated transport mechanism of the maltose ABC importer. *Res. Microbiol.* **2019**, *170*, 321–337. [[CrossRef](#)] [[PubMed](#)]
- Prieß, M.; Göddeke, H.; Groenhof, G.; Schäfer, L.V. Molecular mechanism of ATP hydrolysis in an ABC transporter. *ACS Central Sci.* **2018**, *4*, 1334–1343. [[CrossRef](#)] [[PubMed](#)]
- Brosh, R.M.; Matson, S.W. History of DNA Helicases. *Genes* **2020**, *11*, 255. [[CrossRef](#)]
- Ma, W.; Schulten, K. Mechanism of substrate translocation by a ring-shaped ATPase motor at millisecond resolution. *J. Am. Chem. Soc.* **2015**, *137*, 3031–3040. [[CrossRef](#)]
- Dittrich, M.; Schulten, K. PcrA Helicase, a prototype ATP-driven molecular motor. *Structure* **2006**, *14*, 1345–1353. [[CrossRef](#)]
- Grigorenko, B.L.; Rogov, A.V.; Topol, I.A.; Burt, S.K.; Martinez, H.M.; Nemukhin, A.V. Mechanism of the myosin catalyzed hydrolysis of ATP as rationalized by molecular modeling. *Proc. Natl. Acad. Sci. USA* **2007**, *104*, 7057–7061. [[CrossRef](#)]
- Davidson, R.B.; Hendrix, J.; Geiss, B.J.; Mccullagh, M. Allostery in the dengue virus NS3 helicase: Insights into the NTPase cycle from molecular simulations. *PLoS Comput. Biol.* **2018**, *14*, e1006103. [[CrossRef](#)]
- Geourjon, C.; Orelle, C.; Steinfeld, E.; Blanchet, C.; Deléage, G.; Di Pietro, A.; Jault, J.M. A common mechanism for ATP hydrolysis in ABC transporter and helicase superfamilies. *Trends Biochem. Sci.* **2001**, *26*, 539–544. [[CrossRef](#)]

10. Gardiennet, C.; Schütz, A.K.; Hunkeler, A.; Kunert, B.; Terradot, L.; Böckmann, A.; Meier, B.H. A sedimented sample of a 59 kDa dodecameric helicase yields high-resolution solid-state NMR spectra. *Angew. Chem. Int. Ed.* **2012**, *51*, 7855–7858. [[CrossRef](#)]
11. Wiegand, T.; Lacabanne, D.; Torosyan, A.; Boudet, J.; Cadalbert, R.; Allain, F.H.-T.; Meier, B.H.; Böckmann, A. Sedimentation yields long-term stable protein samples as shown by solid-state NMR. *Front. Mol. Biosci.* **2020**, *7*, 17. [[CrossRef](#)] [[PubMed](#)]
12. Wiegand, T. A solid-state NMR tool box for the investigation of ATP-fueled protein engines. *Prog. Nucl. Magn. Reson. Spectrosc.* **2020**, *117*, 1–32. [[CrossRef](#)] [[PubMed](#)]
13. Takegoshi, K.; Nakamura, S.; Terao, T. <sup>13</sup>C-<sup>13</sup>C polarization transfer by resonant interference recoupling under magic-angle spinning in solid-state NMR. *Chem. Phys. Lett.* **1999**, *307*, 295–302. [[CrossRef](#)]
14. Takegoshi, K.; Nakamura, S.; Terao, T. <sup>13</sup>C-1H dipolar-assisted rotational resonance in magic-angle spinning NMR. *Chem. Phys. Lett.* **2001**, *344*, 631–637. [[CrossRef](#)]
15. Böckmann, A.; Gardiennet, C.; Verel, R.; Hunkeler, A.; Loquet, A.; Pintacuda, G.; Emsley, L.; Meier, B.H.; Lesage, A. Characterization of different water pools in solid-state NMR protein samples. *J. Biomol. NMR* **2009**, *45*, 319–327. [[CrossRef](#)]
16. Cox, N.; Lubitz, W.; Savitsky, A. W-band ELDOR-detected NMR (EDNMR) spectroscopy as a versatile technique for the characterisation of transition metal-ligand interactions. *Mol. Phys.* **2013**, *111*, 2788–2808. [[CrossRef](#)]
17. Cox, N.; Nalepa, A.; Lubitz, W.; Savitsky, A. ELDOR-detected NMR: A general and robust method for electron-nuclear hyperfine spectroscopy? *J. Magn. Reson.* **2017**, *280*, 63–78. [[CrossRef](#)]
18. Goldfarb, D. ELDOR-Detected NMR. In *eMagRes*; Wiley: Hoboken, NJ, USA, 2017; Volume 563, pp. 101–114.
19. Schosseler, P.; Wacker, T.; Schweiger, A. Pulsed ELDOR detected NMR. *Chem. Phys. Lett.* **1994**, *224*, 319–324. [[CrossRef](#)]
20. Giannoulis, A.; Feintuch, A.; Barak, Y.; Mazal, H.; Albeck, S.; Unger, T.; Yang, F.; Su, X.-C.; Goldfarb, D. Two closed ATP- and ADP-dependent conformations in yeast Hsp90 chaperone detected by Mn(II) EPR spectroscopic techniques. *Proc. Natl. Acad. Sci. USA* **2019**, *117*, 395–404. [[CrossRef](#)]
21. Flowers, S.; Biswas, E.E.; Biswas, S.B. Conformational dynamics of DnaB helicase upon DNA and nucleotide-binding: Analysis by intrinsic tryptophan fluorescence quenching. *Biochemistry* **2003**, *42*, 1910–1921. [[CrossRef](#)]
22. Robson, A.; Booth, A.E.; Gold, V.A.; Clarke, A.R.; Collinson, I. A Large conformational change couples the ATP binding site of SecA to the SecY protein channel. *J. Mol. Biol.* **2007**, *374*, 965–976. [[CrossRef](#)] [[PubMed](#)]
23. Orelle, C.; Gubellini, F.; Durand, A.; Marco, S.; Levy, D.; Gros, P.; Di Pietro, A.; Jault, J.-M. Conformational change induced by ATP binding in the multidrug ATP-binding cassette transporter BmrA. *Biochemistry* **2008**, *47*, 2404–2412. [[CrossRef](#)] [[PubMed](#)]
24. Kühner, S.; Fischer, S. Structural mechanism of the ATP-induced dissociation of rigor myosin from actin. *Proc. Natl. Acad. Sci. USA* **2011**, *108*, 7793–7798. [[CrossRef](#)] [[PubMed](#)]
25. Wikström, M. Biophysical and structural aspects of bioenergetics. *R. Soc. Chem.* **2007**, *1*, 414.
26. Chen, B.; Doucleff, M.; Wemmer, D.E.; De Carlo, S.; Huang, H.H.; Nogales, E.; Hoover, T.R.; Kondrashkina, E.; Guo, L.; Nixon, B.T. ATP Ground-and transition states of bacterial enhancer binding AAA+ ATPases support complex formation with their target protein,  $\sigma$ 54. *Structures* **2007**, *15*, 429–440. [[CrossRef](#)]
27. Chabre, M. Aluminofluoride and beryllofluoride complexes: A new phosphate analogs in enzymology. *Trends Biochem. Sci.* **1990**, *15*, 6–10. [[CrossRef](#)]
28. Yount, R.G.; Babcock, D.; Ballantyne, W.; Ojala, D. Adenylyl imidodiphosphate, an adenosine triphosphate analog containing a P-N-P linkage. *Biochemistry* **1971**, *10*, 2484–2489. [[CrossRef](#)]
29. Myers, T.C.; Nakamura, K.; Flesher, J.W. Phosphonic acid analogs of nucleoside phosphates. I. The synthesis of 5'-adenylyl methylenediphosphonate, a phosphonic acid analog of ATP. *J. Am. Chem. Soc.* **2002**, *85*, 3292–3295. [[CrossRef](#)]
30. Goody, R.S.; Eckstein, F. Thiophosphate analogs of nucleoside di- and triphosphates. *J. Am. Chem. Soc.* **1971**, *93*, 6252–6257. [[CrossRef](#)]
31. Mannherz, H.G.; Brehme, H.; Lamp, U. Depolymerisation of F-actin to G-actin and its repolymerisation in the presence of analogs of adenosine triphosphate. *JBIC J. Biol. Inorg. Chem.* **1975**, *60*, 109–116. [[CrossRef](#)]

32. Watanabe, F.; Hashimoto, T.; Tagawa, K. Energy-independent protection of the oxidative phosphorylation capacity of mitochondria against anoxic damage by ATP and its nonmetabolizable analogs<sup>1</sup>. *J. Biochem.* **1985**, *97*, 1229–1234. [[CrossRef](#)] [[PubMed](#)]
33. Suzuki, Y.; Shimizu, T.; Morii, H.; Tanokura, M. Hydrolysis of AMPPNP by the motor domain of ncd, a kinesin-related protein. *FEBS Lett.* **1997**, *409*, 29–32. [[CrossRef](#)]
34. Olesen, C.; Picard, M.; Winther, A.-M.L.; Gyrupe, C.; Morth, J.P.; Oxvig, C.; Møller, J.V.; Nissen, P. The structural basis of calcium transport by the calcium pump. *Nat. Cell Biol.* **2007**, *450*, 1036–1042. [[CrossRef](#)] [[PubMed](#)]
35. Siarheyeva, A.; Liu, R.; Sharom, F.J. Characterization of an asymmetric occluded state of P-glycoprotein with two bound nucleotides. *J. Biol. Chem.* **2010**, *285*, 7575–7586. [[CrossRef](#)] [[PubMed](#)]
36. Ferguson, A.D.; Sheth, P.R.; Basso, A.D.; Paliwal, S.; Gray, K.; Fischmann, T.O.; Le, H.V. Structural basis of CX-4945 binding to human protein kinase CK2. *FEBS Lett.* **2011**, *585*, 104–110. [[CrossRef](#)]
37. Timachi, M.H.; Hutter, C.A.; Hohl, M.; Assafa, T.; Böhm, S.; Mittal, A.; Seeger, M.A.; Bordignon, E. Exploring conformational equilibria of a heterodimeric ABC transporter. *eLife* **2017**, *6*, 257. [[CrossRef](#)]
38. Wiegand, T.; Cadalbert, R.; Gardiennet, C.; Timmins, J.; Terradot, L.; Böckmann, A.; Meier, B.H. Monitoring ssDNA binding to the DnaB helicase from *helicobacter pylori* by solid-state NMR spectroscopy. *Angew. Chem. Int. Ed.* **2016**, *55*, 14164–14168. [[CrossRef](#)]
39. Kung, G.; Runquist, J.A.; Mizioroko, H.M.; Harrison, D.H.T. Identification of the allosteric regulatory site in bacterial phosphoribulokinase. *Biochemistry* **1999**, *38*, 15157–15165. [[CrossRef](#)]
40. Nitta, R.; Kikkawa, M.; Okada, Y.; Hirokawa, N. KIF1A Alternately uses two loops to bind microtubules. *Science* **2004**, *305*, 678–683. [[CrossRef](#)]
41. Reddy, M.C.M.; Palaninathan, S.K.; Shetty, N.D.; Owen, J.L.; Watson, M.D.; Sacchetti, J.C. High resolution crystal structures of Mycobacterium tuberculosis Adenosine Kinase. *J. Biol. Chem.* **2007**, *282*, 27334–27342. [[CrossRef](#)]
42. Shintre, C.A.; Pike, A.C.W.; Li, Q.; Kim, J.-I.; Barr, A.J.; Goubin, S.; Shrestha, L.; Yang, J.; Berridge, G.; Ross, J.; et al. Structures of ABCB10, a human ATP-binding cassette transporter in apo- and nucleotide-bound states. *Proc. Natl. Acad. Sci. USA* **2013**, *110*, 9710–9715. [[CrossRef](#)] [[PubMed](#)]
43. Hassett, A.; Blaettler, W.; Knowles, J.R. Pyruvate kinase: Is the mechanism of phospho transfer associative or dissociative? *Biochemistry* **1982**, *21*, 6335–6340. [[CrossRef](#)]
44. Admiraal, S.J.; Herschlag, D. Mapping the transition state for ATP hydrolysis: Implications for enzymatic catalysis. *Chem. Biol.* **1995**, *2*, 729–739. [[CrossRef](#)]
45. Kamerlin, S.C.L.; Florián, J.; Warshel, A. Associative versus dissociative mechanisms of phosphate monoester hydrolysis: On the interpretation of activation entropies. *ChemPhysChem* **2008**, *9*, 1767–1773. [[CrossRef](#)]
46. Yang, Y.; Cui, Q. The hydrolysis activity of adenosine triphosphate in myosin: A Theoretical analysis of anomeric effects and the nature of the transition state. *J. Phys. Chem. A* **2009**, *113*, 12439–12446. [[CrossRef](#)] [[PubMed](#)]
47. Prasad, B.R.; Plotnikov, N.V.; Warshel, A. Addressing open questions about phosphate hydrolysis pathways by careful free energy mapping. *J. Phys. Chem. B* **2012**, *117*, 153–163. [[CrossRef](#)]
48. Knowles, J.R. Enzyme-catalyzed phosphoryl transfer reactions. *Annu. Rev. Biochem.* **1980**, *49*, 877–919. [[CrossRef](#)]
49. Sondek, J.; Lambright, D.G.; Noel, J.P.; Hamm, H.E.; Sigler, P.B. GTPase mechanism of G proteins from the 1.7-Å crystal structure of transducin  $\alpha$ -GDP AIF-4. *Nat. Cell Biol.* **1994**, *372*, 276–279. [[CrossRef](#)]
50. Wittinghofer, A. Signaling mechanistics: Aluminum fluoride for molecule of the year. *Curr. Biol.* **1997**, *7*, R682–R685. [[CrossRef](#)]
51. Graham, D.L.; Lowe, P.N.; Grime, G.W.; Marsh, M.; Rittinger, K.; Smerdon, S.J.; Gamblin, S.J.; Eccleston, J.F. MgF<sub>3</sub><sup>-</sup> as a transition state analog of phosphoryl transfer. *Chem. Biol.* **2002**, *9*, 375–381. [[CrossRef](#)]
52. Davies, D.R.; Hol, W.G. The power of vanadate in crystallographic investigations of phosphoryl transfer enzymes. *FEBS Lett.* **2004**, *577*, 315–321. [[CrossRef](#)] [[PubMed](#)]
53. Sharma, S.; Davidson, A.L. Vanadate-induced trapping of nucleotides by purified maltose transport complex requires ATP hydrolysis. *J. Bacteriol.* **2000**, *182*, 6570–6576. [[CrossRef](#)] [[PubMed](#)]
54. Loo, T.W.; Clarke, D.M. Vanadate trapping of nucleotide at the ATP-binding sites of human multidrug resistance P-glycoprotein exposes different residues to the drug-binding site. *Proc. Natl. Acad. Sci. USA* **2002**, *99*, 3511–3516. [[CrossRef](#)] [[PubMed](#)]

55. Jin, Y.; Richards, N.G.; Waltho, J.P.; Blackburn, G.M. Metal fluorides as analogues for studies on phosphoryl transfer enzymes. *Angew. Chem. Int. Ed.* **2017**, *56*, 4110–4128. [[CrossRef](#)] [[PubMed](#)]
56. Jin, Y.; Cliff, M.J.; Baxter, N.J.; Dannatt, H.R.W.; Hounslow, A.M.; Bowler, M.W.; Blackburn, G.M.; Waltho, J.P. Charge-balanced metal fluoride complexes for protein kinase a with adenosine diphosphate and substrate peptide SP20. *Angew. Chem. Int. Ed.* **2012**, *51*, 12242–12245. [[CrossRef](#)]
57. Baxter, N.J.; Blackburn, G.M.; Marston, J.P.; Hounslow, A.M.; Cliff, M.J.; Bermel, W.; Williams, N.H.; Hollfelder, F.; Wemmer, A.D.E.; Waltho, J.P. Anionic charge is prioritized over geometry in aluminum and magnesium fluoride transition state analogs of phosphoryl transfer enzymes. *J. Am. Chem. Soc.* **2008**, *130*, 3952–3958. [[CrossRef](#)]
58. Jin, Y.; Molt, R.W.; Blackburn, G.M. Metal fluorides: Tools for structural and computational analysis of phosphoryl transfer enzymes. *Top Curr Chem (Cham)* **2017**, *375*, 1–31. [[CrossRef](#)]
59. Akabayov, S.R.; Akabayov, B. Vanadate in structural biology. *Inorganica Chim. Acta* **2014**, *420*, 16–23. [[CrossRef](#)]
60. Chen, J.; Sharma, S.; Quioco, F.A.; Davidson, A.L. Trapping the transition state of an ATP-binding cassette transporter: Evidence for a concerted mechanism of maltose transport. *Proc. Natl. Acad. Sci. USA* **2001**, *98*, 1525–1530. [[CrossRef](#)]
61. Münnich, S.; Taft, M.H.; Manstein, D.J. Crystal structure of human myosin 1c-The Motor in GLUT4 exocytosis: Implications for Ca<sup>2+</sup> regulation and 14-3-3 binding. *J. Mol. Biol.* **2014**, *426*, 2070–2081. [[CrossRef](#)]
62. Chinthalapudi, K.; Heissler, S.M.; Preller, M.; Sellers, J.R.; Manstein, D.J. Mechanistic insights into the active site and allosteric communication pathways in human nonmuscle myosin-2C. *eLife* **2017**, *6*, e32742. [[CrossRef](#)] [[PubMed](#)]
63. Schmidt, H.; Zalyte, R.; Urnavicius, L.; Carter, A.P. Structure of human cytoplasmic dynein-2 primed for its power stroke. *Nat. Cell Biol.* **2015**, *518*, 435–438. [[CrossRef](#)] [[PubMed](#)]
64. Oldham, M.L.; Chen, J. Snapshots of the maltose transporter during ATP hydrolysis. *Proc. Natl. Acad. Sci. USA* **2011**, *108*, 15152–15156. [[CrossRef](#)] [[PubMed](#)]
65. Hofmann, S.; Januliene, D.; Mehdipour, A.R.; Thomas, C.; Stefan, E.; Brüchert, S.; Kuhn, B.T.; Geertsma, E.R.; Hummer, G.; Tampé, R.; et al. Conformation space of a heterodimeric ABC exporter under turnover conditions. *Nat. Cell Biol.* **2019**, *571*, 580–583. [[CrossRef](#)]
66. Jiang, J.; Maes, E.G.; Taylor, A.B.; Wang, L.; Hinck, A.P.; Lafer, E.M.; Sousa, R. Structural basis of J Cochaperone binding and regulation of Hsp70. *Mol. Cell* **2007**, *28*, 422–433. [[CrossRef](#)]
67. Luo, D.; Xu, T.; Watson, R.P.; Scherer-Becker, D.; Sampath, A.; Jahnke, W.; Yeong, S.S.; Wang, C.H.; Lim, S.P.; Strongin, A.; et al. Insights into RNA unwinding and ATP hydrolysis by the flavivirus NS3 protein. *EMBO J.* **2008**, *27*, 3209–3219. [[CrossRef](#)]
68. Dumais, M.; Davies, D.R.; Lin, T.; Staker, B.L.; Myler, P.J.; Van Voorhis, W.C. Structure and analysis of nucleoside diphosphate kinase from *Borrelia burgdorferi* prepared in a transition-state complex with ADP and vanadate moieties. *Acta Crystallogr. F Struct. Biol. Commun.* **2018**, *74*, 373–384. [[CrossRef](#)]
69. Chen, C.; Saxena, A.K.; Simcoke, W.N.; Garboczi, D.N.; Pedersen, P.L.; Ko, Y.H. Mitochondrial ATP synthase. Crystal structure of the catalytic F1 unit in a vanadate-induced transition-like state and implications for mechanism. *J Biol Chem* **2006**, *281*, 13777–13783. [[CrossRef](#)]
70. Luo, D.; Nakazawa, M.; Yoshida, Y.; Cai, J.; Imai, S. Effects of three different Ca<sub>2+</sub> pump ATPase inhibitors on evoked contractions in rabbit aorta and activities of Ca<sub>2+</sub> pump ATPases in porcine aorta. *Gen. Pharmacol. Vasc. Syst.* **2000**, *34*, 211–220. [[CrossRef](#)]
71. Drakou, C.E.; Malekkou, A.; Hayes, J.M.; Lederer, C.W.; Leonidas, D.; Oikonomakos, N.G.; Lamond, A.I.; Santama, N.; Zographos, S. hCINAP is an atypical mammalian nuclear adenylate kinase with an ATPase motif: Structural and functional studies. *Proteins: Struct. Funct. Bioinform.* **2011**, *80*, 206–220. [[CrossRef](#)]
72. He, C.; Chen, J.; Wang, H.; Wan, Y.; Zhou, J.; Dan, Z.; Zeng, Y.; Xu, W.; Zhu, Y.; Huang, W.; et al. Crystal structures of rice hexokinase 6 with a series of substrates shed light on its enzymatic mechanism. *Biochem. Biophys. Res. Commun.* **2019**, *515*, 614–620. [[CrossRef](#)] [[PubMed](#)]
73. Ho, M.-C.; Shi, W.; Rinaldo-Matthis, A.; Tyler, P.C.; Evans, G.B.; Clinch, K.; Almo, S.C.; Schramm, V.L. Four generations of transition-state analogues for human purine nucleoside phosphorylase. *Proc. Natl. Acad. Sci. USA* **2010**, *107*, 4805–4812. [[CrossRef](#)] [[PubMed](#)]
74. Menz, R.; Walker, J.E.; Leslie, A.G. Structure of bovine mitochondrial F1-ATPase with nucleotide bound to all three catalytic sites. *Cell* **2001**, *106*, 331–341. [[CrossRef](#)]

75. Dinescu, A.; Bhansali, V.S.; Cundari, T.R.; Luo, J.-L.; Anderson, M.E. Function of conserved residues of human glutathione synthetase. *J. Biol. Chem.* **2004**, *279*, 22412–22421. [[CrossRef](#)] [[PubMed](#)]
76. Hunter, T. Why nature chose phosphate to modify proteins. *Philos. Trans. R. Soc. B: Biol. Sci.* **2012**, *367*, 2513–2516. [[CrossRef](#)]
77. Bagshaw, C. ATP analogues at a glance. *J. Cell Sci.* **2001**, *114*, 459–460.
78. Elphick, L.M.; Lee, S.E.; Gouverneur, V.; Mann, D.J. Using chemical genetics and ATP analogues to dissect protein kinase function. *ACS Chem. Biol.* **2007**, *2*, 299–314. [[CrossRef](#)]
79. Wiberg, K. Application of the pople-santry-segal CNDO method to the cyclopropylcarbonyl and cyclobutyl cation and to bicyclobutane. *Tetrahedron* **1968**, *24*, 1083–1096. [[CrossRef](#)]
80. Gardiennet, C.; Wiegand, T.; Bazin, A.; Cadalbert, R.; Kunert, B.; Lacabanne, D.; Gutsche, I.; Terradot, L.; Meier, B.H.; Böckmann, A. Solid-state NMR chemical-shift perturbations indicate domain reorientation of the DnaG primase in the primosome of *Helicobacter pylori*. *J. Biomol. NMR* **2016**, *64*, 189–195. [[CrossRef](#)]
81. Keller, K.; Wiegand, T.; Cadalbert, R.; Meier, B.H.; Böckmann, A.; Jeschke, G.; Yulikov, M. High-spin Metal Centres in Dipolar EPR Spectroscopy. *Chim. Int. J. Chem.* **2018**, *72*, 216–220. [[CrossRef](#)]
82. Wiegand, T.; Cadalbert, R.; Lacabanne, D.; Timmins, J.; Terradot, L.; Böckmann, A.; Meier, B.H. The conformational changes coupling ATP hydrolysis and translocation in a bacterial DnaB helicase. *Nat. Commun.* **2019**, *10*, 1–11. [[CrossRef](#)] [[PubMed](#)]
83. Wiegand, T.; Cadalbert, R.; von Schroetter, C.; Allain, F.H.T.; Meier, B.H. Segmental isotope labelling and solid-state NMR of a 12 × 59 kDa motor protein: Identification of structural variability. *J. Biomol. NMR* **2018**, *71*, 237–245. [[CrossRef](#)] [[PubMed](#)]
84. Wiegand, T.; Gardiennet, C.; Cadalbert, R.; Lacabanne, D.; Kunert, B.; Terradot, L.; Böckmann, A.; Meier, B.H. Variability and conservation of structural domains in divide-and-conquer approaches. *J. Biomol. NMR* **2016**, *65*, 79–86. [[CrossRef](#)] [[PubMed](#)]
85. Wiegand, T.; Gardiennet, C.; Ravotti, F.; Bazin, A.; Kunert, B.; Lacabanne, D.; Cadalbert, R.; Güntert, P.; Terradot, L.; Böckmann, A.; et al. Solid-state NMR sequential assignments of the N-terminal domain of HpDnaB helicase. *Biomol. NMR Assign.* **2015**, *10*, 13–23. [[CrossRef](#)] [[PubMed](#)]
86. Wiegand, T.; Lacabanne, D.; Keller, K.; Cadalbert, R.; Lecoq, L.; Yulikov, M.; Terradot, L.; Jeschke, G.; Meier, B.H.; Böckmann, A. Solid-state NMR and EPR Spectroscopy of Mn<sup>2+</sup>-substituted ATP-fueled protein engines. *Angew. Chem. Int. Ed.* **2017**, *56*, 3369–3373. [[CrossRef](#)]
87. Wiegand, T.; Liao, W.-C.; Ong, T.-C.; Däpp, A.; Cadalbert, R.; Copéret, C.; Böckmann, A.; Meier, B.H. Protein-nucleotide contacts in motor proteins detected by DNP-enhanced solid-state NMR. *J. Biomol. NMR* **2017**, *69*, 157–164. [[CrossRef](#)]
88. Wiegand, T.; Schledorn, M.; Malär, A.A.; Cadalbert, R.; Däpp, A.; Terradot, L.; Meier, B.H.; Böckmann, A. Nucleotide binding modes in a motor protein revealed by <sup>31</sup>P- and <sup>1</sup>H-detected MAS solid-state NMR spectroscopy. *ChemBioChem* **2019**, *21*, 324–330. [[CrossRef](#)]
89. Kunert, B.; Gardiennet, C.; Lacabanne, D.; Calles-Garcia, D.; Falson, P.; Jault, J.-M.; Meier, B.H.; Penin, F.; Böckmann, A.; Böckmann, A. Efficient and stable reconstitution of the ABC transporter BmrA for solid-state NMR studies. *Front. Mol. Biosci.* **2014**, *1*, 5. [[CrossRef](#)]
90. Lacabanne, D.; Kunert, B.; Gardiennet, C.; Meier, B.H.; Böckmann, A. Sample preparation for membrane protein structural studies by solid-state NMR. *Adv. Struct. Saf. Stud.* **2017**, *1635*, 345–358. [[CrossRef](#)]
91. Lacabanne, D.; Lends, A.; Danis, C.; Kunert, B.; Fogeron, M.-L.; Jirasko, V.; Chuilon, C.; Lecoq, L.; Orelle, C.; Chaptal, V.; et al. Gradient reconstitution of membrane proteins for solid-state NMR studies. *J. Biomol. NMR* **2017**, *69*, 81–91. [[CrossRef](#)]
92. Lacabanne, D.; Orelle, C.; Lecoq, L.; Kunert, B.; Chuilon, C.; Wiegand, T.; Ravaud, S.; Jault, J.-M.; Meier, B.H.; Böckmann, A. Flexible-to-rigid transition is central for substrate transport in the ABC transporter BmrA from *Bacillus subtilis*. *Commun. Biol.* **2019**, *2*, 149. [[CrossRef](#)]
93. Aravind, L.; Iyer, L.M.; Leipe, D.D.; Koonin, E.V. A novel family of P-loop NTPases with an unusual phyletic distribution and transmembrane segments inserted within the NTPase domain. *Genome Biol.* **2004**, *5*, R30. [[CrossRef](#)] [[PubMed](#)]
94. Leipe, D.D.; Aravind, L.; Grishin, N.V.; Koonin, E.V. The bacterial replicative helicase DnaB evolved from a RecA duplication. *Genome Res.* **2000**, *10*, 5–16. [[PubMed](#)]
95. Leipe, D.D.; Wolf, Y.I.; Koonin, E.V.; Aravind, L. Classification and evolution of P-loop GTPases and related ATPases. *J. Mol. Biol.* **2002**, *317*, 41–72. [[CrossRef](#)] [[PubMed](#)]

96. Walker, J.; Saraste, M.; Runswick, M.; Gay, N. Distantly related sequences in the alpha- and beta-subunits of ATP synthase, myosin, kinases and other ATP-requiring enzymes and a common nucleotide binding fold. *EMBO J.* **1982**, *1*, 945–951. [[CrossRef](#)]
97. Saraste, M.; Sibbald, P.R.; Wittinghofer, A. The P-loop-A common motif in ATP- and GTP-binding proteins. *Trends Biochem. Sci.* **1990**, *15*, 430–434. [[CrossRef](#)]
98. Iyer, L.M.; Leipe, D.D.; Koonin, E.V.; Aravind, L. Evolutionary history and higher order classification of AAA + ATPases. *J. Struct. Biol.* **2004**, *146*, 11–31. [[CrossRef](#)]
99. Orelle, C.; Dalmas, O.; Gros, P.; Di Pietro, A.; Jault, J.-M. The conserved glutamate residue adjacent to the walker-B motif is the catalytic base for ATP hydrolysis in the ATP-binding cassette transporter BmrA. *J. Biol. Chem.* **2003**, *278*, 47002–47008. [[CrossRef](#)]
100. Feniouk, B.A.; Yoshida, M. Regulatory mechanisms of proton-translocating F(O)F (1)-ATP synthase. *Results Probl. in cell Differ.* **2008**, *45*, 279–308. [[CrossRef](#)]
101. Wittinghofer, A. Phosphoryl transfer in Ras proteins, conclusive or elusive? *Trends Biochem. Sci.* **2006**, *31*, 20–23. [[CrossRef](#)]
102. Wittinghofer, A.; Vetter, I.R. Structure-function relationships of the G Domain, a canonical switch motif. *Annu. Rev. Biochem.* **2011**, *80*, 943–971. [[CrossRef](#)] [[PubMed](#)]
103. Gerwert, K.; Mann, D.; Kötting, C. Common mechanisms of catalysis in small and heterotrimeric GTPases and their respective GAPs. *Biol. Chem.* **2017**, *398*, 523–533. [[CrossRef](#)] [[PubMed](#)]
104. Shalaeva, D.N.; Cherepanov, D.A.; Galperin, M.Y.; Golovin, A.V.; Mulikidjanian, A.Y. Evolution of cation binding in the active sites of P-loop nucleoside triphosphatases in relation to the basic catalytic mechanism. *Elife* **2018**, *7*, e37373e. [[CrossRef](#)]
105. Wilkens, S. Structure and mechanism of ABC transporters. *F1000Prime Rep.* **2015**, *7*, 14. [[CrossRef](#)] [[PubMed](#)]
106. Ford, R.C.; Beis, K. Learning the ABCs one at a time: Structure and mechanism of ABC transporters. *Biochem. Soc. Trans.* **2019**, *47*, 23–36. [[CrossRef](#)]
107. Ogawa, T.; Saijo, S.; Shimizu, N.; Jiang, X.; Hirokawa, N. Mechanism of catalytic microtubule depolymerization via KIF2-tubulin transitional conformation. *Cell Rep.* **2017**, *20*, 2626–2638. [[CrossRef](#)]
108. Steinfels, E.; Orelle, C.; Fantino, J.-R.; Dalmas, O.; Rigaud, J.-L.; Denizot, F.; Di Pietro, A.; Jault, J.-M. Characterization of YvcC (BmrA), a multidrug ABC transporter constitutively expressed in *Bacillus subtilis*. *Biochemistry* **2004**, *43*, 7491–7502. [[CrossRef](#)]
109. Tomblin, G.; Senior, A.E. The occluded nucleotide conformation of P-glycoprotein. *J. Bioenerg. Biomembr.* **2005**, *37*, 497–500. [[CrossRef](#)]
110. Van Veen, H.W.; Margolles, A.; Müller, M.; Higgins, C.F.; Konings, W.N. The homodimeric ATP-binding cassette transporter LmrA mediates multidrug transport by an alternating two-site (two-cylinder engine) mechanism. *EMBO J.* **2000**, *19*, 2503–2514. [[CrossRef](#)]
111. Orelle, C.; Jault, J.-M. Structures and transport mechanisms of the ABC efflux pumps. In *Efflux-Mediated Antimicrobial Resistance in Bacteria*; Springer Science and Business Media LLC: Basel, Switzerland, 2016; pp. 73–98.
112. Collauto, A.; Mishra, S.; Litvinov, A.; Mchaourab, H.S.; Goldfarb, D. Direct spectroscopic detection of ATP turnover reveals mechanistic divergence of ABC exporters. *Structure* **2017**, *25*, 1264–1274.e3. [[CrossRef](#)]
113. Soni, R.K.; Mehra, P.; Choudhury, N.R.; Mukhopadhyay, G.; Dhar, S.K. Functional characterization of *Helicobacter pylori* DnaB helicase. *Nucleic Acids Research* **2003**, *31*, 6828–6840. [[CrossRef](#)] [[PubMed](#)]
114. Lapina, O.; Shubin, A.; Khabibulin, D.; Terskikh, V.V.; Bodart, P.; Amoureux, J.-P. Solid-state NMR for characterization of vanadium-containing systems. *Catal. Today* **2003**, *78*, 91–104. [[CrossRef](#)]
115. Fernandez, C.; Bodart, P.; Amoureux, J.-P. Determination of 51V quadrupole and chemical shift tensor orientations in V2O5 by analysis of magic-angle spinning nuclear magnetic resonance spectra. *Solid State Nucl. Magn. Reson.* **1994**, *3*, 79–91. [[CrossRef](#)]
116. Rehder, D.; Polenova, T.; Buhl, M. Vanadium-51 NMR. In *Annual Reports on NMR Spectroscopy*; Elsevier BV: Amsterdam, The Netherlands, 2007; Volume 62, pp. 49–114.
117. Aureliano, M.; Tiago, T.; Gândara, R.M.; Sousa, A.; Moderno, A.; Kaliva, M.; Salifoglou, A.; Duarte, R.O.; Moura, J.J.G. Interactions of vanadium(V)-citrate complexes with the sarcoplasmic reticulum calcium pump. *J. Inorg. Biochem.* **2005**, *99*, 2355–2361. [[CrossRef](#)]
118. Fenn, A.; Wächtler, M.; Gutmann, T.; Breitzke, H.; Buchholz, A.; Lippold, I.; Plass, W.; Buntkowsky, G. Correlations between 51V solid-state NMR parameters and chemical structure of vanadium (V) complexes as

- models for related metalloproteins and catalysts. *Solid State Nucl. Magn. Reson.* **2009**, *36*, 192–201. [[CrossRef](#)] [[PubMed](#)]
119. Pooransingh-Margolis, N.; Renirie, R.; Hasan, Z.; Wever, R.; Vega, A.J.; Polenova, T. 51V solid-state magic angle spinning NMR spectroscopy of vanadium chloroperoxidase. *J. Am. Chem. Soc.* **2006**, *128*, 5190–5208. [[CrossRef](#)]
120. McCann, N.; Wagner, M.; Hasse, H. A thermodynamic model for vanadate in aqueous solution-equilibria and reaction enthalpies. *Dalton Trans.* **2013**, *42*, 2622–2628. [[CrossRef](#)] [[PubMed](#)]
121. Iannuzzi, M.; Young, T.; Frankel, G.S. Aluminum alloy corrosion inhibition by vanadates. *J. Electrochem. Soc.* **2006**, *153*, B533–B541. [[CrossRef](#)]
122. Lewinson, O.; Orelle, C.; Seeger, M.A. Structures of ABC transporters: Handle with care. *FEBS Letters* **2020**. [[CrossRef](#)]
123. Müller, B. *ChemEQL Version 3.2*; Swiss Federal Institute of Aquatic Science and Technology: Kastanienbaum, Switzerland, 2015.
124. Bao, H.; Dalal, K.; Cytrynbaum, E.N.; Duong, F. Sequential action of MalE and maltose allows coupling ATP hydrolysis to translocation in the MalFGK2 transporter. *J. Biol. Chem.* **2015**, *290*, 25452–25460. [[CrossRef](#)]
125. Mehmood, S.; Domene, C.; Forest, E.; Jault, J.-M. Dynamics of a bacterial multidrug ABC transporter in the inward-and outward-facing conformations. *Proc. Natl. Acad. Sci. USA* **2012**, *109*, 10832–10836. [[CrossRef](#)] [[PubMed](#)]
126. Singleton, M.R.; Sawaya, M.R.; Ellenberger, T.; Wigley, D.B. Crystal structure of T7 gene 4 ring helicase indicates a mechanism for sequential hydrolysis of nucleotides. *Cell* **2000**, *101*, 589–600. [[CrossRef](#)]
127. Bailey, S.; Eliason, W.K.; Steitz, T.A. Structure of hexameric DnaB helicase and its complex with a domain of DnaG primase. *Science* **2007**, *318*, 459–463. [[CrossRef](#)] [[PubMed](#)]
128. Singleton, M.R.; Dillingham, M.S.; Wigley, D.B. Structure and mechanism of helicases and nucleic acid translocases. *Annu. Rev. Biochem.* **2007**, *76*, 23–50. [[CrossRef](#)] [[PubMed](#)]
129. Enemark, E.J.; Joshua-Tor, L. On helicases and other motor proteins. *Curr. Opin. Struct. Biol.* **2008**, *18*, 243–257. [[CrossRef](#)]
130. Wang, G.; Klein, M.G.; Tokonzaba, E.; Zhang, Y.; Holden, L.G.; Chen, X.S. The structure of a DnaB-family replicative helicase and its interactions with primase. *Nat. Struct. Mol. Biol.* **2007**, *15*, 94–100. [[CrossRef](#)]
131. Itsathiphaisarn, O.; Wing, R.A.; Eliason, W.K.; Wang, J.; Steitz, T.A. The hexameric helicase DnaB adopts a nonplanar conformation during translocation. *Cell* **2012**, *151*, 267–277. [[CrossRef](#)]
132. Gao, Y.; Cui, Y.; Fox, T.; Lin, S.; Wang, H.; De Val, N.; Zhou, Z.H.; Yang, W. Structures and operating principles of the replisome. *Science* **2019**, *363*, eaav7003. [[CrossRef](#)]
133. Gordon, J.A. Use of vanadate as protein-phosphotyrosine phosphatase inhibitor. In *Methods in Enzymology*; Academic Press: San Diego, CA, USA, 1991; Volume 201, pp. 477–482.
134. Gor'kov, P.L.; Witter, R.; Chekmenev, E.Y.; Nozirov, F.; Fu, R.; Brey, W.W. Low-E probe for (19)F-(1)H NMR of dilute biological solids. *J. Magn. Reson.* **2007**, *189*, 182–189. [[CrossRef](#)]
135. Fogh, R.; Ionides, J.; Ulrich, E.; Boucher, W.; Vranken, W.; Linge, J.P.; Habeck, M.; Rieping, W.; Bhat, T.N.; Westbrook, J.; et al. The CCPN project: An interim report on a data model for the NMR community. *Nat. Struct. Biol.* **2002**, *9*, 416–418. [[CrossRef](#)]
136. Stevens, T.J.; Fogh, R.H.; Boucher, W.; Higman, V.A.; Eisenmenger, F.; Bardiaux, B.; van Rossum, B.J.; Oschkinat, H.; Laue, E.D. A software framework for analysing solid-state MAS NMR data. *J. Biomol. NMR* **2011**, *51*, 437–447. [[CrossRef](#)] [[PubMed](#)]
137. Vranken, W.F.; Boucher, W.; Stevens, T.J.; Fogh, R.H.; Pajon, A.; Llinas, M.; Ulrich, E.L.; Markley, J.L.; Ionides, J.; Laue, E.D. The CCPN data model for NMR spectroscopy: Development of a software pipeline. *Proteins* **2005**, *59*, 687–696. [[CrossRef](#)] [[PubMed](#)]

**Publisher's Note:** MDPI stays neutral with regard to jurisdictional claims in published maps and institutional affiliations.



© 2020 by the authors. Licensee MDPI, Basel, Switzerland. This article is an open access article distributed under the terms and conditions of the Creative Commons Attribution (CC BY) license (<http://creativecommons.org/licenses/by/4.0/>).